Hyperbolic wavelet power spectra of nonstationary signals

Khoa N. Le*
Kishor P. Dabke
Gregory K. Egan
Monash University
Clayton Campus
Department of Electrical and Computer Systems Engineering
Melbourne, Australia
E-mail: Khoa.Le@eng.monash.edu.au

Abstract. The hyperbolic kernel and hyperbolic wavelet were shown to be useful and effective in time-frequency signal processing (Le et al., 2001 and 2003). We introduce the time-frequency wavelet power spectrum as a useful technique to study signal characteristics in which the hyperbolic and sym3 wavelets are employed. The hyperbolic wavelet power spectrum technique is employed for signals including electrocardiogram (ECG), sinusoidal, transient exponential, music, and speech. Comparisons between the Fourier power spectrum technique and hyperbolic wavelet power spectrum technique are also made. [DOI: 10.1117/1.1608002]

Subject terms: time-frequency hyperbolic wavelet power spectrum; wavelet transform; Fourier transform; power spectrum; Duffing chaos; electrocardiogram; music; speech.

Paper 020469 received Oct. 25, 2002; revised manuscript received Feb. 26, 2003; accepted for publication Apr. 9, 2003.

1 Theoretical Background of the Wavelet Power Spectrum Technique

Fourier transform and Fourier power spectral techniques have been employed to analyze signals for many years. In particular, the power spectrum and bispectrum have been successfully used to study chaos and signal behavior in Refs. 1–7. Note that the Fourier power spectral technique is optimally used when the signal is statistically invariant, i.e., for stationary signals. Mathematically, the Fourier transform, power spectrum, and bispectrum of an input signal $x(t)$ are given as[10]

$$\hat{X}(\omega)=\int_{-\infty}^{+\infty}x(t)\exp(-j\omega t)\mathrm{d}t, \tag{1}$$

$$P(\omega)=\hat{X}(\omega)\hat{X}^*(\omega)=|\hat{X}(\omega)|^2, \tag{2}$$

$$B(\omega_1,\omega_2)=\hat{X}(\omega_1)\hat{X}(\omega_2)\hat{X}^*(\omega_1+\omega_2), \tag{3}$$

where $x(t)$ is the input signal, $\hat{X}(\omega)$ is its Fourier transform, $P(\omega)$ is the power spectrum, $B(\omega_1,\omega_2)$ is the bispectrum, and ω is a frequency variable in radians per-second.

When the signal is nonstationary, time-frequency power spectral and wavelet transform techniques should be employed. The short-time Fourier transform (STFT) has been employed to study nonstationary signals with great success.[8] However, there is a trade-off between time and frequency resolutions since the STFT uses a window to "slice" the signal waveform to smaller segments and each segment is approximately assumed to be stationary. This can be identified as the major disadvantage of the STFT. The time-frequency power spectrum and the wavelet transform have been successfully shown to be useful tools to study multicomponent nonstationary signals in Refs. 8–20. All time-frequency power spectra are governed by the general Cohen equation, which is given by[8,20]

$$P(t,\omega)=\frac{1}{4\pi^2}\int_{-\infty}^{+\infty}\int_{-\infty}^{+\infty}\int_{-\infty}^{+\infty}\exp(-j\theta t-j\tau\omega+j\theta u)\times\Phi(\theta,\tau)R_{t,1}(t,\tau)\mathrm{d}u\,\mathrm{d}\tau\,\mathrm{d}\theta, \tag{4}$$

where $R_{t,1}(t,\tau)$ is the local autocorrelation function, $\Phi(\theta,\tau)$ is the kernel function, $u=t+\tau/2$, τ is the lag parameter, and t is the running time variable. The range of t is $0\leq t\leq t_0$, where t_0 is the signal window size over which the power spectrum of a nonstationary signal is estimated.

The STFT has been studied extensively in Ref. 8, therefore, the main purpose of the paper is not comparing the STFT with the new hyperbolic wavelet power spectrum (WPS) technique of various signals. Instead, this paper presents early results on signal analysis by using the new technique. Further quantitative work on the new technique will be presented in future publications. The wavelet transform (WT) of an input signal $x(t)$ is given by[17]

$$\mathrm{WT}(a,b)=\int_{-\infty}^{+\infty}x(t)\psi\left(\frac{t-b}{a}\right)\mathrm{d}t, \tag{5}$$

where $\psi(t-b/a)$ is the wavelet function, and a and b are scale and time indices, respectively. To be a valid wavelet, a function must have a zero area under its curve. This condition is satisfied by all sinusoids including sym3 and the hyperbolic wavelet, which is given by

*Present address: Griffith University, School of Engineering, Gold Coast, Parklands Drive, Southport QLD 4215, Australia; e-mail: K.Le@griffith.edu.au.

$$\psi_{\mathrm{Hy}}(\theta)=(-1)n\beta^2[\mathrm{sech}(\beta\theta)]^n\{n-(n+1)[\mathrm{sech}(\beta\theta)]^2\}, \quad (6)$$

where β is a control parameter that can be varied. Further work on the hyperbolic wavelet and other symmetrical wavelets can be found in Ref. 21.

van Milligen et al.[22,23] showed how the WPS and wavelet bispectral techniques were used to study chaos and turbulence, which provide the foundation for the research reported in this paper. In their studies, they showed that the wavelet bispectrum could be utilized to effectively study chaos. They showed that the main problem with the wavelet bispectrum was that there are four dimensions that must be simultaneously expressed. Thus, the concept of slicing the wavelet bispectrum at different separate frequencies was employed, which was shown to be successful provided that the behavior of the signal could be partially predicted. Farge et al.[12] showed that the WT method could be used to study turbulence by detecting edgy behavior in its time-frequency spectrum. Similar to the Fourier power spectrum and bispectrum, the WPS and bispectrum are given by

$$\mathrm{WPS}(t,\omega)=\mathrm{WT}(t,\omega)\mathrm{WT}^*(t,\omega)=|\mathrm{WT}(t,\omega)|^2, \quad (7)$$

$$\mathrm{WPS}(t,\omega)=\mathrm{WT}(t,\omega_1)\mathrm{WT}(t,\omega_2)\mathrm{WT}[t,(\omega_1+\omega_2)]. \quad (8)$$

The WPS technique is much simpler than the wavelet bispectrum technique since there are only three quantities, i.e., time, scale, and magnitude, that must be simultaneously displayed. One major advantage of the WPS technique over the Fourier power spectrum technique is that the signal energy distribution is shown in 3-D graphs, which do not suppress the phase information as is the case of the power spectrum, i.e., the phase information is included as a function of time. Jubran et al.[24] used the Gaussian WT to study the behavior of flow-induced vibration and cross-flow in a cylinder. They compared the performance of a number of different mother wavelets including the Morlet wavelet, Daubechies wavelets, and the Gaussian wavelet, and then concluded that the Gaussian wavelet was the most suitable wavelet for this particular application. In that paper, only the WT of the input data was estimated, while the WPS and bispectrum techniques were not considered.

The main difference between the WT and the Fourier transform is that the WT examines the frequency contents of the signal over a short time period since its mother wavelet function has finite-time support. By contrast, the Fourier transform averages the frequency contents of the signal over an infinite time interval by the effects of $\sin(\cdot)$ and $\cos(\cdot)$ functions. The time-support range of most wavelet functions (the hyperbolic, the Choi-Williams, or Mexican-hat and Morlet wavelets, for example) is an approximately 10- to 20-unit time index (as was seen in Ref. 21). Thus, by employing the WT, it is possible to observe instantaneous behavior of the signal, which is vital in studying the signal characteristics and predicting its future behavior. In addition, the WPS technique gives the energy density of the input signal in both the time and frequency domains, whereas the Fourier power spectrum displays the energy contents of the signal in the frequency domain only. The combination of time and frequency domains yields local images of the input signal energy contents and thus it is possible to carry out an in-depth study of the signal by examining its instantaneous behavior. Since many different wavelet functions exist, the corresponding WTs also exist and each wavelet function has different characteristics, which means that they can be used for different specific applications. The hyperbolic wavelet function, which was proposed in Ref. 21, is employed in this paper to further demonstrate the usefulness of the hyperbolic kernel family. The hyperbolic wavelet has been shown to have a fine scale resolution, which is suitable for studying signals that do not have broad power spectra such as transients, which was concluded in Ref. 21. The hyperbolic wavelet function also has a small number of computed scales, which means it can be used for compression purposes, which reduces the computational burden of the hyperbolic wavelet power spectrum.

The main aim of this paper is to first demonstrate that the hyperbolic WPS technique is a valid and effective technique to study nonstationary signals. The sym3 WPS technique and Fourier power spectral techniques are employed solely to qualitatively show the hyperbolic wavelet effectiveness and validity in signal processing. Second, the paper qualitatively presents early results on the main characteristics of a number of important signals including electrocardiogram (ECG), music, Duffing chaotic oscillator, and speech. Quantitative studies on these signals using the new technique, especially the ECG, which has potential in medical applications, and quantitative comparisons of the hyperbolic WPS technique with other techniques such as STFT will be presented in future publications and therefore are not strongly emphasized in the paper. The main reason that the sym3 wavelet is used in conjunction with the hyperbolic wavelet is that it is a simple and symmetrical wavelet. Therefore, quantitative comparisons between the two wavelets are not strongly emphasized in this work, which appears to be qualitative. Furthermore, other wavelets could be used to successfully validate the hyperbolic wavelet. However, we believe that the sym3 wavelet is a well-chosen wavelet. Unlike the work done by Milligen and others, the work reported in this paper explores further the effectiveness and usefulness of the WPS technique using the hyperbolic wavelet by studying instantaneous behavior and energy distributions of nonstationary signals. The paper is organized as follows. The WPS of a periodic sinusoidal signal is studied first in Sec. 2 as this is the most common and well-known signal in signal processing. Section 3 examines the popular exponential signal $\exp(-t)$. Section 4 calculates the WPS of an exponentially decaying sinusoid $\sin(t)\exp(-t)$. The Duffing oscillator is studied in Sec. 5 including periods 1, 2, and 4 and the chaotic state. Section 6 shows that the hyperbolic WPS technique can be used to study the ECG qualitatively. Sections 7 and 8 examine music and speech waveforms. The Fourier power spectra of these signals are also given to validate results drawn by using the hyperbolic WPS technique.

2 WPS of a Sinusoid

In this section, contour plots of $\mathrm{WPS}_{\mathrm{sym3}}$ and $\mathrm{WPS}_{\mathrm{hyp}}$ of a periodic sinusoid $\sin(2\pi t)$ are given in Figs. 1 and 2, respectively, in which periodicity can be identified by the following points:

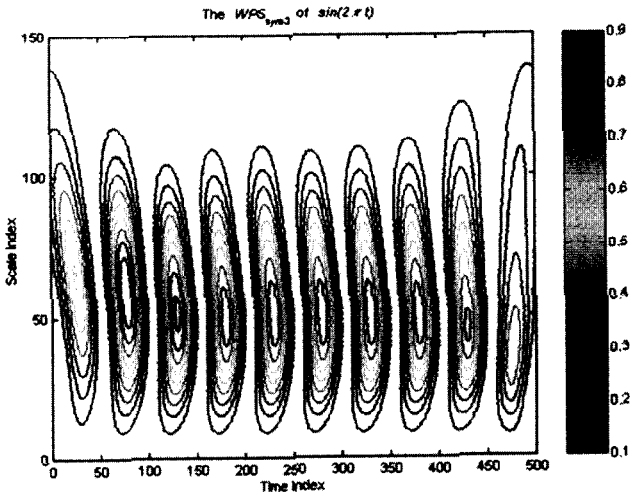

Fig. 1 Contour plot of the WPS_{sym3} of a $\sin(2\pi t)$ signal.

1. There is a clear boundary between the peaks of the signal, which indicates strong periodic behavior. In addition, the energy is mainly concentrated at harmonic peaks and there is no broad energy distribution over a wide scale range. The harmonic peaks are located at the approximate scale of $a \approx 50$.
2. Contour curves are closely spaced and there are a large number of bounded small-radius contours toward the harmonic peaks.
3. The energy is discretely and uniformly distributed. The most important and recognizable feature of a periodic signal is that its energy distribution is repetitive. It can be seen that the discrete peaks of the input signal are clearly displayed by the WPS technique. Thus, it is evident that for periodic signals, their wavelet power spectra are not broad and smeared but discontinuous and exhibit distinctive peaks.

The WPS_{hyp} in Fig. 2 shows distinctive peaks, which indicate strong periodic behavior of the signal, as expected.

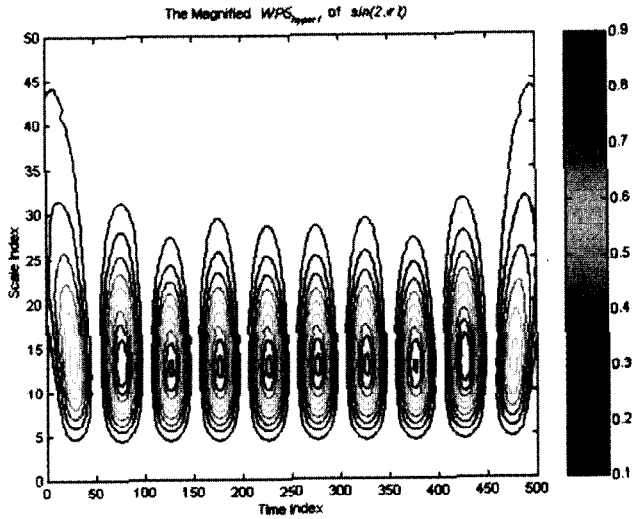

Fig. 2 Contour plot of the WPS_{hyp} of a $\sin(2\pi t)$ signal.

Compared with the WPS_{sym3} given in Fig. 1, the WPS_{hyp} requires a smaller number of scales, which improves the computational efficiency of the hyperbolic time-frequency power spectrum. From Figs. 1 and 2, the scale ranges of a harmonic peak using the sym3 and hyperbolic wavelets are approximately $20 \leq a_{sym3} \leq 130$ and $5 \leq a_{hyp} \leq 45$ respectively, where a_{sym3} and a_{hyp} are the scale indices of the sym3 and hyperbolic wavelets, respectively. As we can see, the WPS_{sym3} and WPS_{hyp} are consistent, which validates the hyperbolic wavelet and therefore the hyperbolic WPS technique.

The relationship between the center scale a_{center} and the frequency of the signal f_{signal} is given by[25]

$$a_{center} = \frac{f_{samp}\omega_0}{2\pi f_{wsamp}} \frac{1}{f_{signal}} \quad \text{or} \quad f_{signal} = \frac{f_{samp}\omega_0}{2\pi f_{wsamp}} \cdot \frac{1}{a_{center}}, \tag{9}$$

where f_{wsamp}, f_{samp}, and ω_0 are the wavelet sampling frequency, the sampling frequency of the signal, and the center frequency of the wavelet, respectively. Note that the center frequency is the center of the innermost eclipse contour with the highest scale.

From Eq. (9), the signal frequency f_{signal} can be estimated based on the center scale a_{center} specified by the WPS. The sampling frequency of the signal f_{samp} is usually about 100 times larger than the wavelet sampling frequency f_{wsamp}, since the number of required sampling points for a wavelet function is much smaller than that for a signal, as discussed in Ref. 21. For a sinusoidal input signal of $\sin(2\pi t)$, using the sym3 wavelet with the center frequency $\omega_0 = 3$ rad/s, $a_{center} \approx 50$, Fig. 1 and Eq. (9), the signal frequency f_{signal} can be approximately estimated as

$$f_{signal} \approx \frac{(100)(3)}{2\pi} \frac{1}{50} \approx 0.96 \text{ Hz}. \tag{10}$$

Similarly, the signal frequency f_{signal} of the signal $\sin(2\pi t)$ can be approximately estimated using the hyperbolic wavelet with the center frequency $\omega_0 = \beta = 1$ rad/s, $a_{center} \approx 13$, Fig. 2, and Eq. (9), we obtain

$$f_{signal} \approx \frac{(100)(1)}{2\pi} \frac{1}{13} \approx 1.2 \text{ Hz}. \tag{11}$$

From the calculations performed in Eqs. (10) and (11), it is clear that the frequency of the signal can be estimated. Note that the percent error could be as high as 20% [Eq. (11)] as in the case of the hyperbolic wavelet. Thus, quantitatively, the signal frequency can be more accurately estimated by using the Fourier power spectrum technique.

3 WPS of an Exponential Transient Signal

Exponential signals are common responses of first- and second-order linear circuits. This is the main reason why it is included in this research. The WPS_{sym3} of a transient signal $\exp(-t)$ is given in Fig. 3.

The WPS_{sym3} of an exponential signal $\exp(-t)$ is broad and there seems to exist one distinctive peak represented by the smallest-radius contour curve with a large contour scale

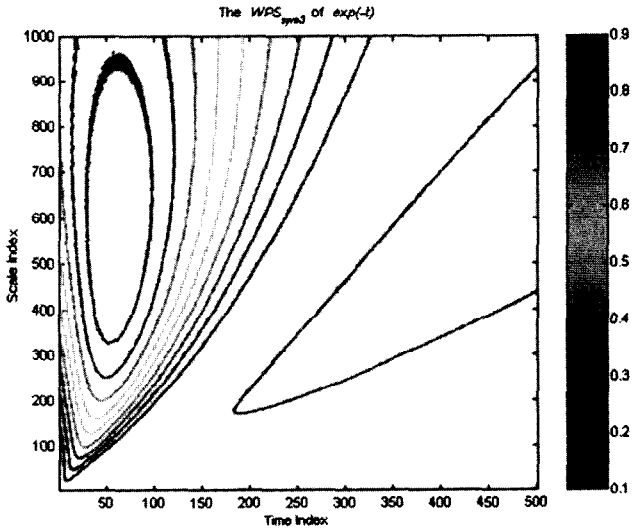

Fig. 3 Contour plot of the WPS_{sym3} of the $\exp(-t)$ signal.

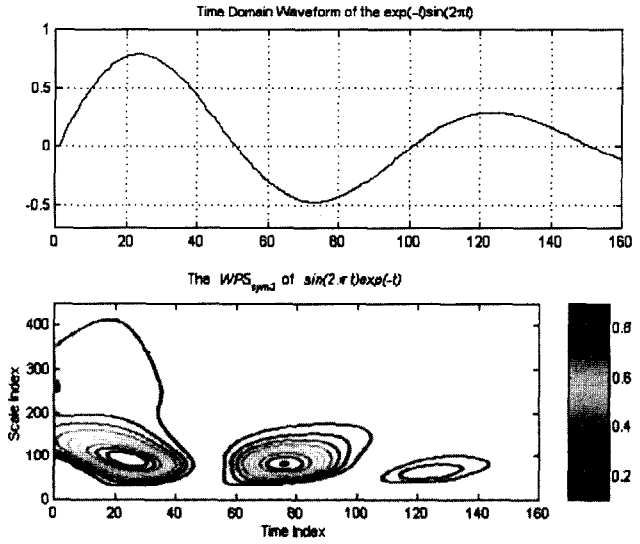

Fig. 5 Time-domain waveform and contour plot of the WPS_{sym3} of an exponentially decaying sinusoid $\exp(-t)\sin(2\pi t)$. The WPS_{hyp} is very similar to the WPS_{sym3}.

in Fig. 3. The contour plot of the exponential transient signal is not closely spaced, as it was in the case of a sinusoid. In fact, the number of closed contours is less than that of the sinusoid even though they both have dominant peak(s). The decay rate or time constant of the exponential signal is approximately the scale difference between the centers of two adjacent contours. From Fig. 3, the scale difference between the innermost contour curve and the second innermost curve is about 60, which corresponds to the decay rate of 0.8 by using Eq. (9). The accuracy of the estimation can be improved by taking the scale-difference average of all adjacent-contour pairs, which yields the time constant of about 0.99. This is the expected time constant of the investigated exponential signal. Note that the energy of an exponential signal is not concentrated at one particular scale, but instead, spreads over a wide scale range, as can be seen in Fig. 3. The exponential energy tends to form closed contours, but this process appears to be very slow, i.e., contour curves have nearly infinitely large radii, which reflect the nature of exponential transient signals. The WPS_{hyp} is given in Fig. 4.

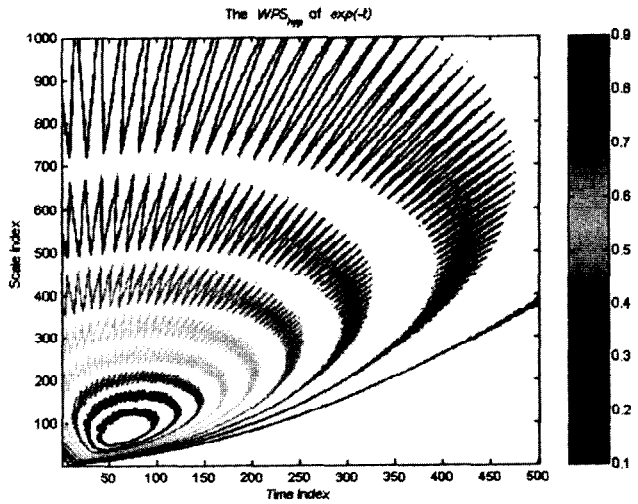

Fig. 4 Contour plot of the WPS_{hyp} of an $\exp(-t)$ signal.

The time constant of the exponential signal can be similarly estimated using the same method applied to the hyperbolic wavelet. From Fig. 4, the scale difference between two innermost adjacent contour curves is approximately 20, which corresponds to the time constant of 0.78. By taking the scale-difference average, we obtain the estimated time constant of the exponential signal of about 0.95, which is close to the expected result. Even though the time constant of a transient signal can be estimated with reasonable precision, it is still hard to estimate since the center of each contour curve is sometimes hard to determine. For example, for the case of the sym3 wavelet, since the centers of all contour curves cannot be clearly displayed, the distance between two adjacent curves along the vertical line is taken instead. For the hyperbolic wavelet, since most of the curves are clearly displayed, the scale difference between two adjacent centers can be effectively estimated. Second, this process is lengthy and tedious since the average value of the scale differences of all contour curves must be calculated. The WPS_{hyp} in Fig. 4 is consistent with the WPS_{sym3} given in Fig. 3, in which large-radius contours are detected. The peak is detected by the smallest contour curve. Even though the peak contour curve has a high scale, it is not filled, which illustrates the main difference between sinusoidal signals and exponential signals. For the former, all peak contour curves are filled, whereas that is not the case for the latter. If the contour curves are filled, then the signal energy tends to be more concentrated around the peak, which implies periodic characteristics. Note also that the WPS_{hyp} is calculated over a smaller scale range than that of the WPS_{sym3}.

4 WPS of an Exponentially Decaying Sinusoidal Signal

This section examines the WPS of an exponentially decaying sinusoidal signal $\exp(-t)\sin(2\pi t)$. The periodic and

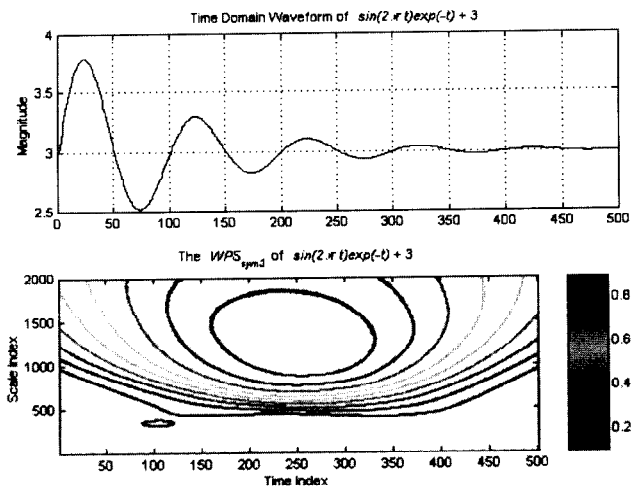

Fig. 6 Contour plot of the WPS_{sym3} of the $\sin(2\pi t)\exp(-t)+3$ signal.

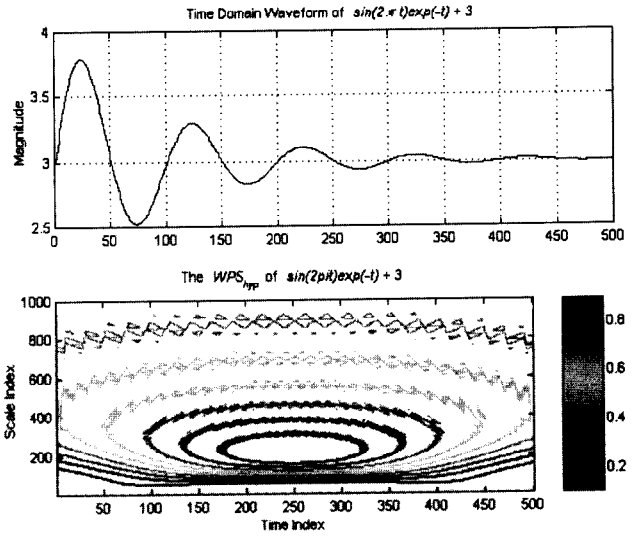

Fig. 7 Time-domain waveform and contour plot of the WPS_{hyp} of the $\sin(2\pi t)\exp(-t)+3$ signal.

transient components of this signal were separately studied in Secs. 2 and 3, respectively. The contour plot of its WPS_{sym3} is given in Fig. 5. The WPS_{hyp} is similar to the WPS_{sym3} and is not given in this case.

It is expected that this signal has a combination of transient and periodic characteristics, which hopefully can be detected by the WPS technique. From Fig. 5, it is evident that the energy density is densely concentrated at the scale of about 100 for three harmonic peaks and decays to 0 as the signal reaches steady state. There are three dominant and distinctive peaks in the signal, whose positions correspond to those shown by the time-domain waveform. These peaks are clearly detected by using the WPS technique and indicated by three closed contours, which represent periodic characteristics of the signal. The diminishing of energy as the signal reaches steady state indicates that the final value of the signal is 0. Note also that the number of contour curves surrounding the peaks decreases as the time index increases, which reflects transient characteristics in the signal. In particular, the number of contour curves in the third peak is only two at low scales compared with nine curves at high scales for the first and second peaks. Thus, it might be suggested that exponentially decaying sinusoidal signals with a zero final value can be well recognized by using the WPS technique. If the final value of an exponentially decaying sinusoidal signal is nonzero, its WPS is expected to be broad since the peaks are now smoothened by a broad energy distribution of the dc component.[26] As a result, the WPS of an exponentially decaying sinusoid with a nonzero final value has only one major peak whose contours are not closely spaced, as can be seen in Fig. 6. Note that the transient characteristics of the signal are indicated by large-radius contour curves, as was seen in Sec. 3 for the case of an exponential signal. The main difference between an exponentially decaying sinusoid with a nonzero final value and an exponential signal is that for the former, the radii of energy contours are not infinitely large but finite. This reflects periodic characteristics in the former signal whose WPS tends to form islands of closed contour curves. For comparison purposes, the WPS_{hyp} of the signal $\sin(2\pi t)\exp(-t)+3$ is shown in Fig. 7.

From Fig. 7, the upper parts of the contour curves have thick edges, which indicate an energy-smearing phenomenon. It should not be incorrectly concluded that the signal is chaotic since the contour curves are densely located in the time-frequency plane, which indicates discrete energy distribution. These features enable distinctive differentiation between exponentially decaying sinusoids with a nonzero final value and chaotic signals such as the ECG, which is examined later. The scale ranges in Figs. 6 and 7 are different since the WPS_{hyp} in Fig. 7 is magnified so that its contour curves can be clearly displayed. It is clear that the hyperbolic wavelet is more efficient than the sym3 wavelet in which more contour curves are displayed over the same scale range. In Ref. 21, it was reported that the hyperbolic wavelet is most suitable for transient signals. By comparing Figs. 6 and 7, it is clear that the WPS_{hyp} can display more contour curves than the WPS_{sym3} due to the fact that the former has a finer scale resolution and a smaller total number of calculated scales. This fact was also shown in Ref. 21 when calculating the hyperbolic, Morlet and Choi-Williams wavelet power spectra of the English vowel "e". In addition, by comparing Figs. 3 and 4 and Figs. 6 and 7, it might be suggested that the hyperbolic wavelet is a symmetrical function whose wavelet power spectra are perfectly symmetrical about the vertical line. Thus, graphical representations of the hyperbolic wavelet power spectra are better displayed than using the sym3 wavelet. As a result, it is easier to differentiate the exponential signal from the exponentially decaying sinusoidal signals with zero and nonzero values by using the hyperbolic WPS. Further, one advantage of the hyperbolic wavelet over the sym3 wavelet is that the former can reveal more information over an identical scale range than the latter due to the compression ability of the hyperbolic wavelet of having a smaller total number of calculated scales. This also increases the efficiency of the hyperbolic WPS calculation process.

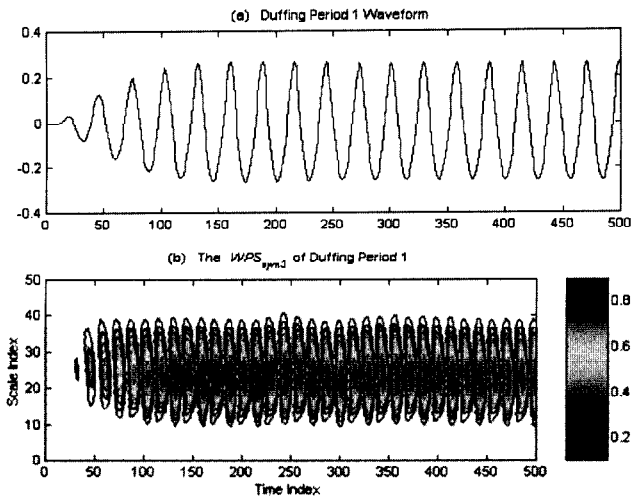

Fig. 8 Time-domain waveform and contour plot of the WPS_{sym3} of Duffing period 1. The WPS_{hyp} of a Duffing period 1 waveform is very similar to the WPS_{sym3} except that it is displayed on a different scale range.

5 WPS of the Duffing Oscillator

The Duffing oscillator has been popular in signal processing because of its simplicity.[6] In this section, the Duffing oscillator is studied by calculating its wavelet power spectra of periods 1, 2, and 4 and the chaotic state. From this, it is possible to determine how its energy is distributed and therefore deduce the system characteristics and detect possible transition(s) into the chaotic region. The equation governing Duffing oscillator is given as[6]

$$\ddot{u}+\gamma\dot{u}-0.5(u-u^3)=F\cos(\omega t), \tag{12}$$

where $\gamma=0.168$, $\omega=1$, $u(t)$ is the displacement function of the time t, and F is the driving function. For period 1, $F_1=0.05$; for period 2, $F_2=0.178$; for period 4, $F_4=0.197$; and for the chaotic state, $F_{chaos}=0.21$. The initial conditions used for the system were $[u\ \dot{u}]=[0\ 1]$.

5.1 *Duffing Period 1*

A Duffing period 1 waveform can be regarded as a genuine periodic signal whose energy is concentrated over the high-frequency range (low-scale range). A Duffing period 1 time-domain waveform and its WPS using the hyperbolic and sym3 wavelets are given in Fig. 8. Note that the energy is uniformly and repetitively distributed over the whole range of the time index, which means each segment of the input data points is almost identical. This means that there is no degree of disorder or chaos in a Duffing period 1 waveform.

From Fig. 8, periodic (harmonic) peaks of the Duffing period 1 waveform are clearly separated, which is similar to the case of the sinusoidal signal $\sin(t)$ studied in Sec. 2. Apart from a minor drift of the signal at the beginning where the time index is roughly $b\leqslant 300$, there is no difference in the amount of energy density over time, which suggests that a Duffing period 1 waveform is nearly periodic. The duration during which the periodic peak occupies is short, which suggests that the signal energy is highly concentrated. This fact has been well known and extensively reported in the literature.[6] Thus the correctness and consistency of the proposed WPS technique are validated.

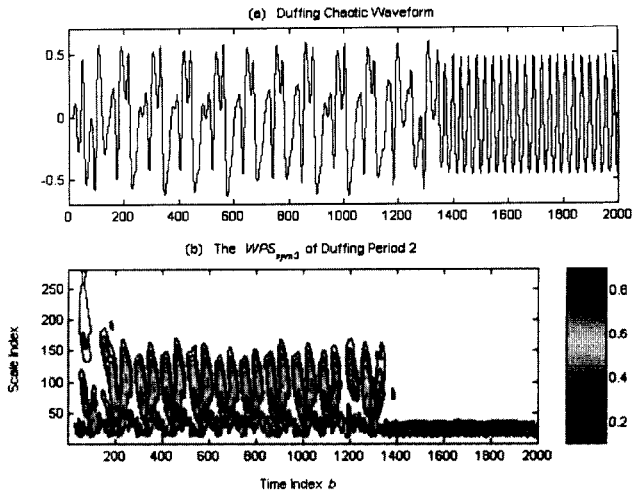

Fig. 9 Time-domain waveform of a Duffing period 2 and contour plot of its WPS_{sym3}.

5.2 *Duffing Period 2*

The driving force used for the Duffing period 2 waveform in Eq. (12) is $F_2=0.178$. The time-domain waveform and its WPS_{sym3} are displayed in Fig. 9. The WPS_{hyp} of a Duffing period 2 waveform is given in Fig. 10.

The time-domain waveform of Duffing period 2 shows an early sign of deviation from periodicity in which the number of detected subharmonics is large. The signal regains its near-periodic characteristics at the time index $b\approx 1400$. For $b\geqslant 1400$, the signal exhibits similar characteristics to those of the Duffing period 1 waveform, which suggests that periodicity is dominant. However, since its contour scale is lower than that of the Duffing period 1 waveform, it can be suggested that the Duffing period 2 waveform does not completely regain its periodicity, as can

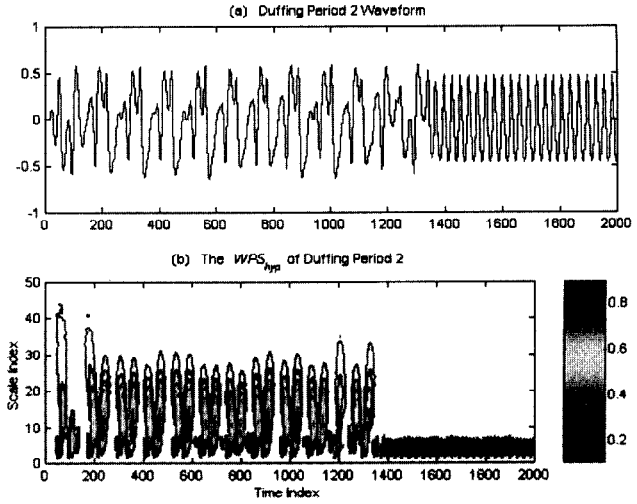

Fig. 10 Time-domain waveform and contour plot of the WPS_{hyp} of the Duffing period 2.

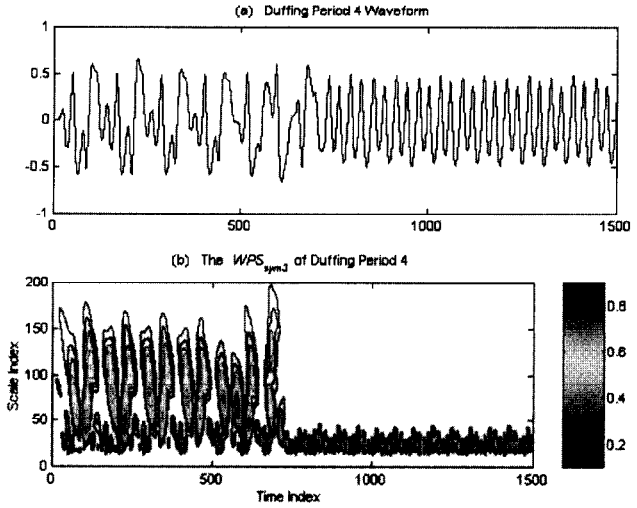

Fig. 11 Duffing period 4 time-domain waveform and contour plot of its WPS_{sym3}.

be seen in Fig. 9. The near periodicity of a Duffing period 2 waveform is detected by a series of closed and filled contours (at high scales) with repetitive patterns over time. Although there are discrete and filled contours, more subharmonics are detected by the WPS technique in a Duffing period 2 waveform than in a Duffing period 1 waveform. In addition, the contour scale of the WPS of a Duffing period 2 waveform is lower than that of a Duffing period 1 waveform, which suggests that the former has a broader energy distribution than that of the latter.

Note that the WPS_{sym3} and WPS_{hyp} are consistent and can be employed to successfully detect periodicity and deviation from periodicity of the Duffing period 2 waveform.

5.3 *Duffing Period 4*

A Duffing period 4 waveform can be regarded as a transition state from periodicity to chaos,[6] which hopefully will

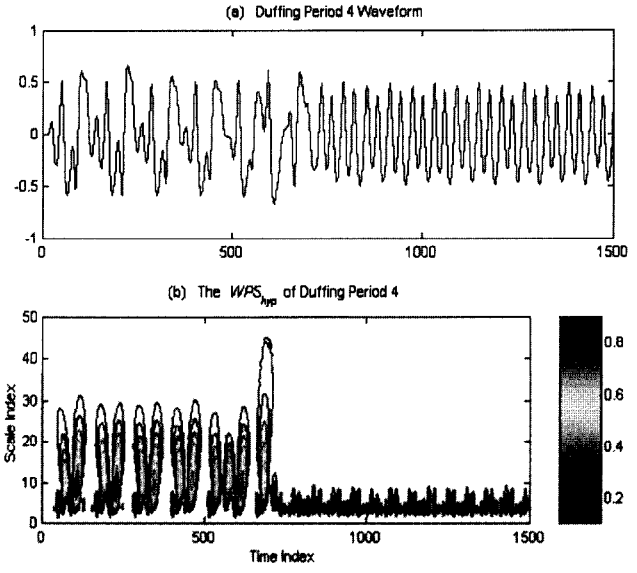

Fig. 12 Time-domain waveform and contour plot of the WPS_{hyp} of Duffing Period 4.

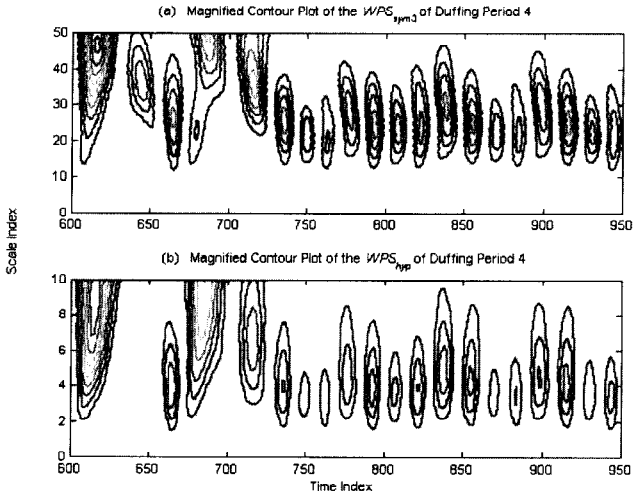

Fig. 13 Magnified contour plots of the WPS_{sym3} and WPS_{hyp} of a Duffing period 4 waveform, which shows the transition into the chaotic region at $b \approx 700$. For $b \geq 700$, the Duffing period 4 waveform partially regains its periodicity by having repetitive closed contour curves. However, these curves have low contour scales, which suggests that their energy is not densely distributed. Thus, the waveform is vulnerable to chaotic behavior.

be detected by using the WPS technique. The time-domain waveform and its WPS_{sym3} of a Duffing period 4 waveform are given in Fig. 11. The WPS_{hyp} is given in Fig. 12.

Similar to the Duffing period 2 waveform, the Duffing period 4 waveform exhibits early deviation from periodicity with two major harmonics and a number of subharmonics for $b \leq 700$. Transitions into the chaotic region is signaled by continuous closed contours at $b \approx 700$ with a wider scale range, as can be seen in Fig. 11. The continuity of energy indicates that the waveform has entered into the chaotic region. However, chaotic components of the waveform are not strong enough since periodic components are still present. For $b \geq 700$, the signal partially regains its periodicity with low-contour-scale curves. All of the preceding features can be clearly seen in the magnified contour plots of the WPS_{sym3} and WPS_{hyp} shown in Fig. 13. From Figs. 11 and 12, it can be seen that the hyperbolic and sym3 wavelet power spectra of a Duffing period 4 waveform are consistent in which the transition into the chaotic region is detected at $b \approx 700$. For $b < 700$, near-periodic behavior is detected in the waveform, and for $b > 700$ a mixture of chaotic and periodic components are detected. However, due to the compression effects of the hyperbolic wavelet, some subharmonics are suppressed. Note that by using the WPS time-frequency technique, it is possible to determine when the waveform enters into the chaotic region hence the transition region of the waveform can be clearly identified.

5.4 *Duffing Chaos*

For a Duffing chaotic waveform, the driving force has the value of $F_{chaos} = 0.21$. The time-domain waveform and its WPS_{sym3} are shown in Fig. 14. The WPS_{hyp} is given in Fig. 15. The magnified versions of these figures are given in Figs. 16 and 17, respectively.

From Figs. 14 and 15, a Duffing chaotic waveform exhibits early deviation from periodicity as was detected in

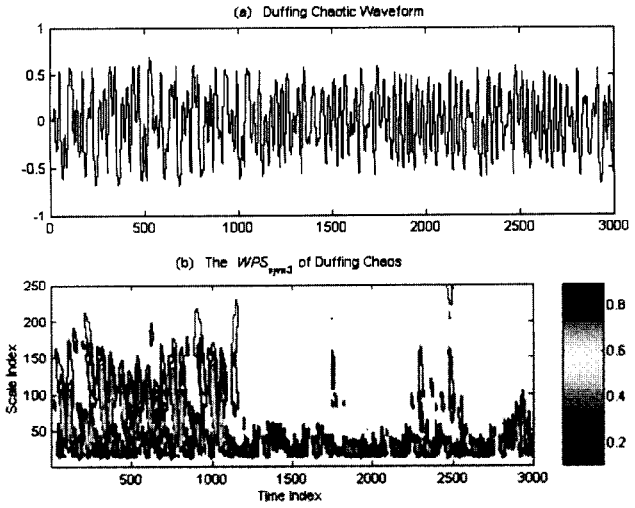

Fig. 14 Time-domain waveform of Duffing chaos and contour plot of its WPS_{sym3}.

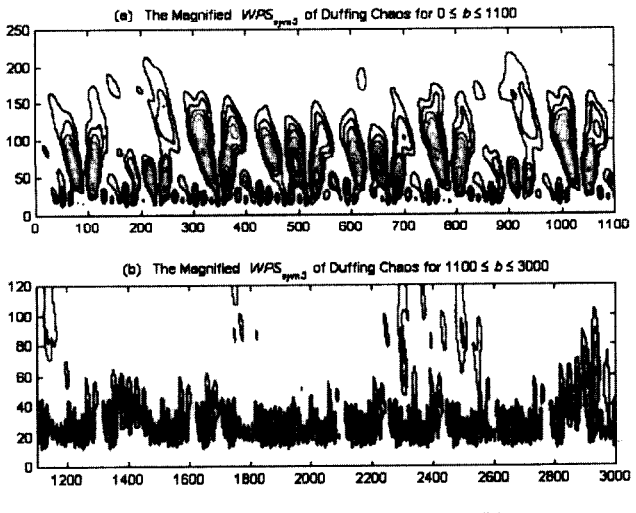

Fig. 16 Magnified version of Fig. 14(b).

Duffing period 2 and 4 waveforms. However, instead of regaining its periodicity, the Duffing chaotic waveform remains chaotic after the transition into its chaotic region. The Duffing chaotic state is signaled by a nonrepetitive and broad energy distribution in which distinctive peaks are unevenly distributed for a time index less than 1100, which is the transition region of the waveform. All of these features can be seen in Figs. 16(a) and 17(a). From Figs. 14 and 16, for a time index greater than 1100, it is evident that the waveform has entirely entered into the chaotic state in which its fundamental periodic components have disappeared as compared to Duffing period 1, 2, and 4 waveforms. The energy is unevenly distributed over the scale range of 20 to 250. There is no particular energy concentration in any region of the spectrum (due to low contour scales), which is broadly distributed [approximately at the time indices of 1100, 1700 and 2500 in Fig. 15(b)], which strongly suggests that the waveform is chaotic. Note that in this case, even though the curves have low contour scales, they still represent repetitive energy patterns, which means that for a time index greater than 1100, a Duffing chaotic waveform still possesses weak periodicity. Thus, it can be suggested that a Duffing chaotic waveform is superposition of periodic and chaotic components. The main difference between a Duffing period 4 waveform and a Duffing chaotic waveform is that there are no disordered energy patterns in the former, whereas the contour scales of the latter vary with time, which suggests disordered characteristics. Figures 16(b) and 17(b) clearly show the magnified energy distribution of the waveform for a time index greater than 1100.

6 WPS of ECG Signal

The practical ECG (human electrocardiogram) is examined in this section due to its importance in medical diagnosis. The hyperbolic wavelet power spectrum is used to study the ECG with the prime purpose of revealing its chaotic nature. The work in this paper presents early results on basic characteristics of the ECG by using the hyperbolic WPS technique. Thus this section does not deal with the ECG from a medical point of view. Further studies are done to show that the hyperbolic WPS can provide quantitative

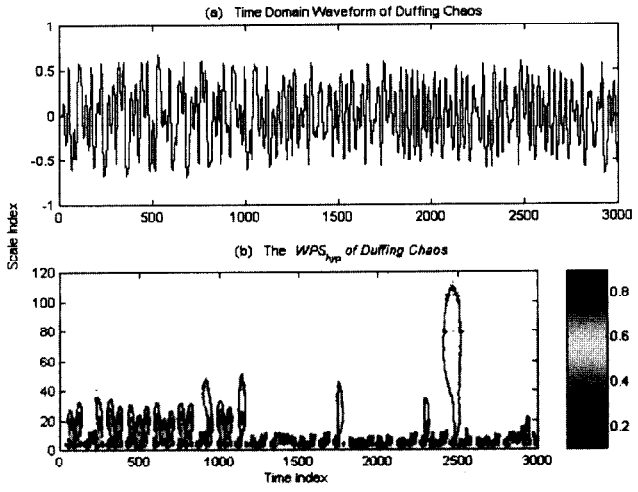

Fig. 15 Time-domain waveform and contour plot of the WPS_{hyp} of Duffing chaos.

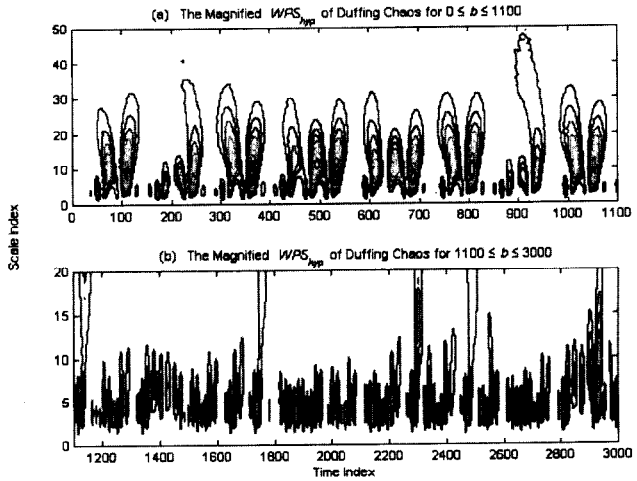

Fig. 17 Magnified version of Fig. 15(b).

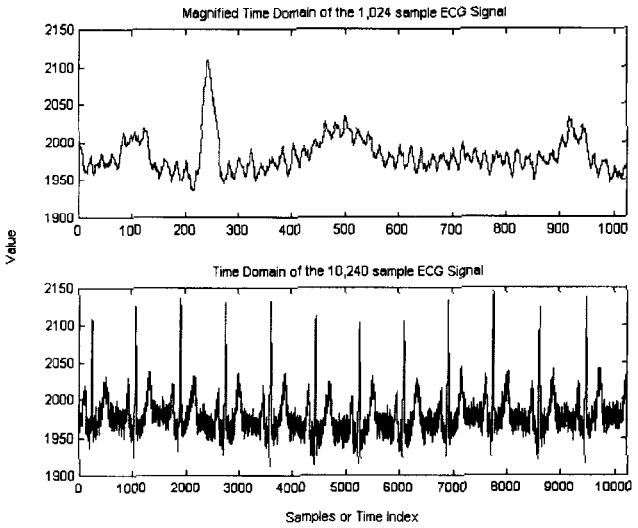

Fig. 18 Time-domain waveform of an ECG.

details from the ECG, which are valuable for predicting patients symptoms. The ECG has also been studied extensively in Refs. 16 and 27–29 using time-frequency techniques and the bispectrum.[3]

The time-domain waveform of the ECG signal is displayed in Fig. 18. The WPS_{sym3} of an ECG signal, which is shown in Fig. 19 in a 3-D plot and in Fig. 20 in a contour plot, is similar to that of the exponential signal shown in Sec. 3 and quite similar to the WPS_{sym3} of the exponentially decaying sinusoid with a nonzero dc component shown in Sec. 4. For periodic and exponentially decaying sinusoidal signals, their WPSs all have dominant peaks and large-radius contours. The WPS_{sym3} of the ECG does not have identifiable peaks and its contours have very large radii, which suggests that the ECG might be a transient type. The energy distribution of the ECG is spread over a wide scale range, as can be seen in Fig. 20. In addition, ECG contours are not sharp but thick in width. The scale range of contour curves is worked out by estimating the corresponding scales of the lowest and the highest contours. For example, in Fig. 20, the scale range of the sym3

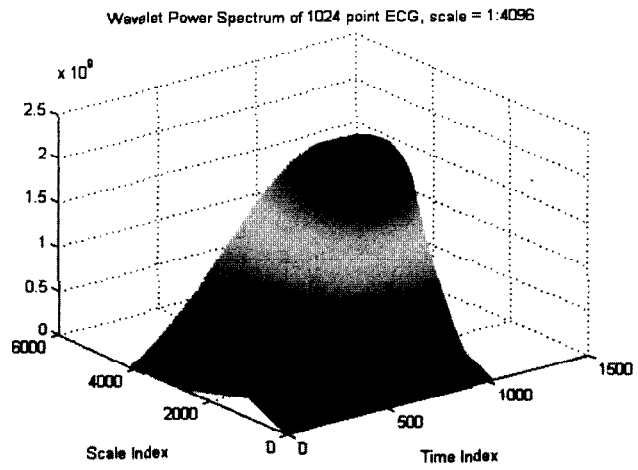

Fig. 19 3-D mesh plot of the WPS_{sym3} of a 1024-point ECG.

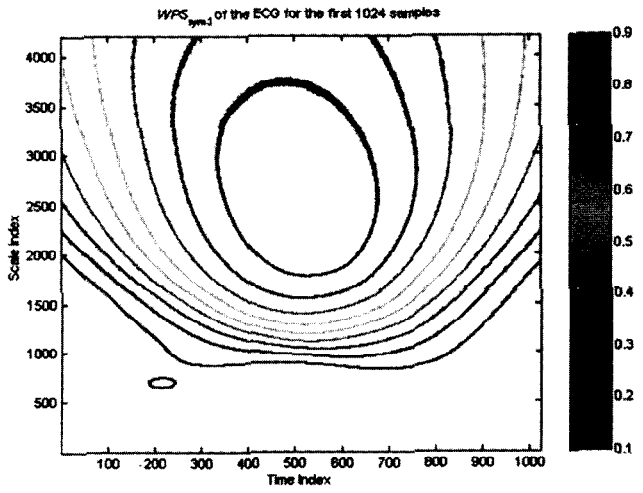

Fig. 20 Contour plot of the WPS_{sym3} of a 1024-point ECG signal.

wavelet power spectrum will be $900 \leqslant a$, not $2000 \leqslant a$, since the lower contour stretches down to the scale of 900 and 2000 is its starting point. This method was used in this paper to work out the scale range of various WPSs. From Fig. 19, the ECG energy distribution is smooth and there are no abrupt changes in its energy density over the high- and low-valued region of the scale and time indices. By comparing the WPS_{sym3} in Fig. 6 (the exponentially decaying sinusoid with a nonzero final value) and Fig. 20 (ECG signal), it is evident that the energy density of the ECG is broader and distributed over a larger scale range of $900 \leqslant a \leqslant 3500$ than that of an exponentially decaying sinusoid with a nonzero dc component ($500 \leqslant a \leqslant 1800$).

In addition, the innermost contour curve has the scale range of $1800 \leqslant a \leqslant 3700$ for the ECG and $900 \leqslant a \leqslant 1800$ (smaller scale range than the ECG) for the exponential signal, which suggests that the former might exhibit chaotic characteristics. However, since the energy patterns provided by the WPS technique are almost similar, it is difficult to distinguish between these signals.

For comparison purposes, the WPS_{hyp} is shown in Fig. 21, in which it is symmetrically displayed about the vertical

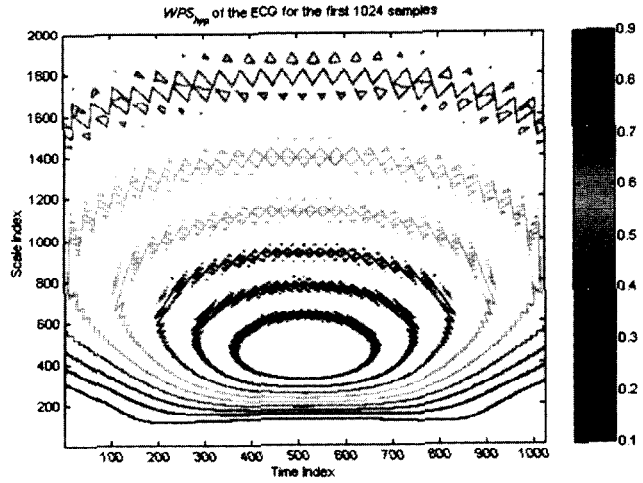

Fig. 21 Contour plot of the WPS_{hyp} of an ECG.

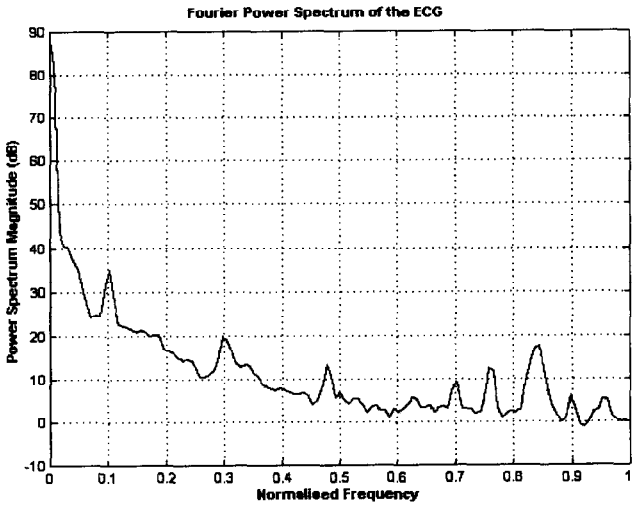

Fig. 22 Fourier power spectrum of an ECG signal. The frequency is normalized by dividing every frequency bin by the largest frequency bin in the signal spectrum.

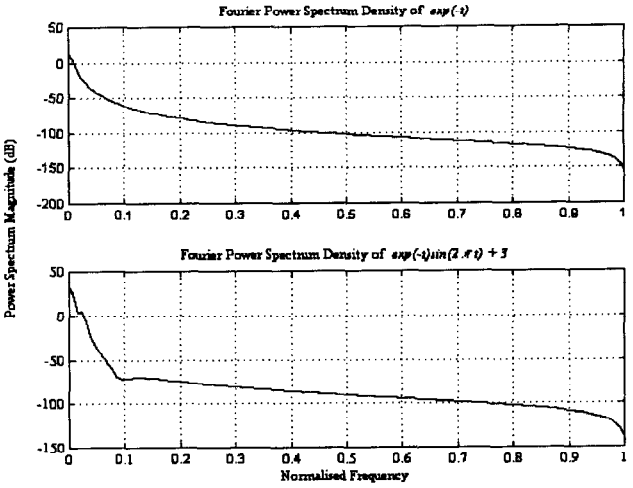

Fig. 23 Fourier power spectra of $\exp(-t)$ and $\exp(-t)\sin(t)+3$ signals.

axis at the time index $b=500$. The center of the eclipse with the highest scale is located at $(a,b)=(500,500)$ on the time-scale plane, as can be seen in Fig. 21. From Sec. 4 the $\mathrm{WPS}_{\mathrm{hyp}}$ of an exponentially decaying sinusoid with a nonzero final value is very similar to that of the ECG. The only difference between the two WPSs is that the occupied scale range of the ECG ($120 \leqslant a \leqslant 1800$ in Fig. 21) is wider than that of an exponentially decaying sinusoidal signal with a nonzero final value ($70 \leqslant a \leqslant 850$ in Fig. 7). This suggests that the ECG energy distribution is broader than that of the exponentially decaying sinusoid signal, as explained earlier. In addition, the WPS of the exponential signal has more contour curves over the same scale range than those of the ECG WPS, which further supports the preceding statement.

The scale ranges of the ECG and an exponentially sinusoidal signals, using the hyperbolic wavelet, are clearly different compared with those observed using the near-symmetric sym3 wavelet, which makes the differentiation of these signals easier. This indicates the usefulness of a perfectly symmetrical wavelet such as the hyperbolic wavelet. Thus, the hyperbolic wavelet power spectrum technique can be used to study the ECG signal by examining the occupied scale range of its WPS. In general, however, the WPS technique is not very effective in studying the ECG signal since it cannot clearly differentiate between an exponentially decaying signal and the ECG signal due to their identical WPSs. This is a disadvantage of the WPS technique compared with the Fourier power spectrum technique. Although the WPSs of the ECG and $\exp(-t)\sin(t)+3$ signals are very similar, their Fourier power spectra, given in Figs. 22 and 23, respectively, are quite different, which shows that the Fourier technique is more effective than the WPS technique in this case. Thus, depending on the particular application, the WPS technique or the Fourier power spectrum technique should be used to reveal the signal characteristics. In this case, it might be suggested that the ECG signal can be effectively studied using the Fourier power spectrum technique. This conclusion is consistent with the findings in Ref. 3. From Fig. 22, it is evident that the ECG signal has a broad power spectrum, which suggests that it is not periodic. This is consistent with the conclusions drawn by using the WPS technique from Figs. 19 to 21. The transient characteristics of the ECG signal, however, are not effectively detected by using the Fourier power spectrum technique, but can be detected by using the WPS technique.

From Fig. 23, there is a minor discrepancy with the magnitude of the power spectrum of the $f(t)=\exp(-t)\sin(t)+3$ signal at dc condition. The power of the signal $[f(t)]^2$ at dc condition is 9, which corresponds to about $10\log_{10}(9.0)\approx 9.5$ dB. The signal power calculated by MATLAB gives a value of about 30 dB. To work out the power at a dc condition, we take the magnitude of the power spectrum at dc, which is 30 dB, and divide that by $\sqrt{2\pi}$, which yields about 12 dB. This corresponds to a percent age error of about 26% with respect to 9.5 dB. Note that this method of power spectral estimation by MATLAB is only approximate. In addition, it is the qualitative information of the graph that is of importance, not the quantitative details. However, to provide a satisfactory result, the Welch method of power spectral estimation can be used to obtain the power spectrum of the signal. This method yields the dc power of about 9.6 dB, which corresponds to about 0.1% error. However, calculation of the Fourier power spectra of signals is not the main emphasis of this paper and we stop the discussion about power spectral estimation at this point. Table 1 summarizes notable characteristics of an exponential signal $\exp(-t)$, an exponentially decaying sinusoidal signal with a zero final value $\exp(-t)\sin(t)$, an exponentially decaying sinusoidal signal with a nonzero final value $\exp(-t)\sin(t)+3$, and the ECG signal.

Throughout this paper, comparisons between the hyperbolic and sym3 WPSs have been made. It can be seen that the $\mathrm{WPS}_{\mathrm{hyp}}$ of most signals have a smaller scale range than that of the $\mathrm{WPS}_{\mathrm{sym3}}$, which significantly reduces the WPS computational burden. In addition, the $\mathrm{WPS}_{\mathrm{hyp}}$ converges faster than the $\mathrm{WPS}_{\mathrm{sym3}}$ in the case of an exponential signal in which the signal energy distribution is more clearly displayed by using the hyperbolic wavelet than by using the

Table 1 Characteristics of $\exp(-t)$, $\exp(-t)\sin(t)$, $\exp(-t)\sin(t)+3$, and ECG signals.

Signal	Characteristics
$\exp(-t)$	Exhibits transient behavior, periodicity is not present, bounded energy.
$\sin(t)\exp(-t)$	Exhibits transient and periodic behavior, strong sinusoidal decaying characteristics, bounded energy, WPS contour curves have small radii; energy smearing is not present.
$\sin(t)\exp(-t)+3$	Exhibits transient behavior, bounded energy due to closed contour curves. The density of contour curves is high, which suggests that the signal is not chaotic. WPS contour curves have large radii; energy smearing is not present.
ECG	Exhibits transient and chaotic behavior, bounded energy, WPS contour curves have large radii, energy smearing is present. The occupied WPS scale range of the ECG signal is wider than that of the $\sin(t)\exp(-t)+3$ signal.

sym3 wavelet. One advantage of the WPS_{sym3} over the WPS_{hyp} is that the former can clearly display all subharmonics of signals, whereas, some subharmonics are missing if the latter is used due to the compression effects[21] as is also demonstrated in the following sections. This can be seen as a trade-off between efficiency and fine-detail display of the hyperbolic and sym3 wavelets.

7 WPSs of Music

Music signals are studied in detail using the hyperbolic WPS technique. Musical sounds have been studied by a number of researchers on music multidimensional scale analysis,[30–32] music classification,[33–36] music identification,[37] and music recognition by using the continuous wavelet transform.[38] Classifying different piano sounds was studied by Delf and Jondral by using a number of time-frequency techniques such as the STFT and the Wigner-Ville time-frequency distribution. Hamdy et al.[34] and Lambrou et al.[35] reported a music classification method using a statistical technique of calculating skewness; entropy; and the first- and second-order statistics of different musical sounds such as jazz, rock, pop and then estimated the appropriate threshold so that these sounds can be clearly distinguished. The main limitation of this method is that it does not make use of the instantaneous information of the signal, which yields its characteristics and hence enables effective signal classification. Olmo et al.[38] designed the new wavelet, called the log-Morlet wavelet, then showed that the new wavelet was capable of recognizing different harmonics and tones in music waveforms by using the continuous WT. This method used the same principle in detecting edges and abrupt changes in an input signal as was reported in Ref. 14. The main difference of this work from our work is that we employ the hyperbolic WPS for music recognition and to study music characteristics. Although time and frequency localization was employed in Ref. 38, it was not as strongly emphasised as in this paper. In particular, all harmonics and subharmonics will be identified in both time and frequency domains, which enables effective music recognition. Note that a harmonic peak can be identified by having a color contour scale of larger than

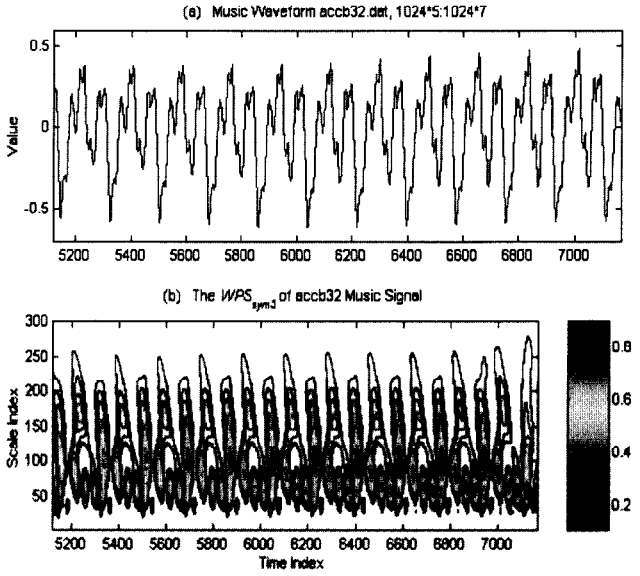

Fig. 24 Time-domain waveform and contour plot of the WPS_{sym3} of the accordion music; data samples are in the range of 1024 $\times$5:1024$\times$7.

0.7 and a subharmonic peak that has a contour scale of smaller than 0.7, but usually, it is less than 0.5. The lower the order of a subharmonic, the lower the contour scale. This method was also employed by Olmo et al.[38] and Sussaman and Karsh[36] by means of energy separation. The terms "harmonic" and "subharmonic" describe behavior of the signal at specific scales given the locations of wavelet coefficients on contour graphs. These terms are used because of their popularity in signal processing.

7.1 *WPS of an Accordion Music Signal*

Various segments of the accordion music signal are examined in this section so that its instantaneous behavior can be detected. For data samples from 1024$\times$5 to 1024$\times$7 and from 1024$\times$30 to 1024$\times$32, the WPSs of each set are given in Figs. 24 and 25, respectively.

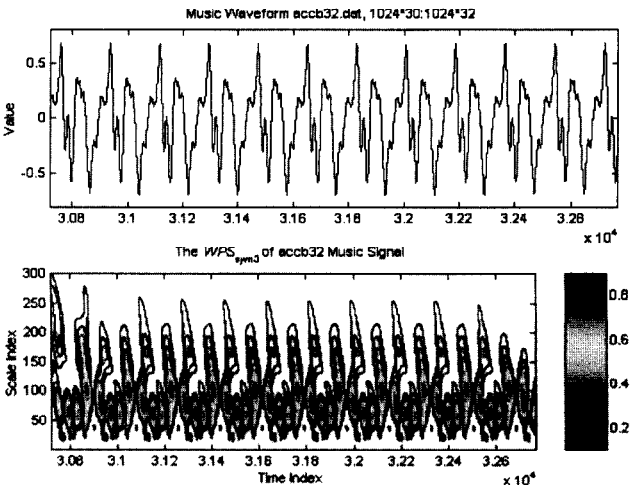

Fig. 25 Time-domain waveform and contour plot of the WPS_{sym3} of the accordion music signal for data samples from 30$\times$1024 to 32 $\times$1024.

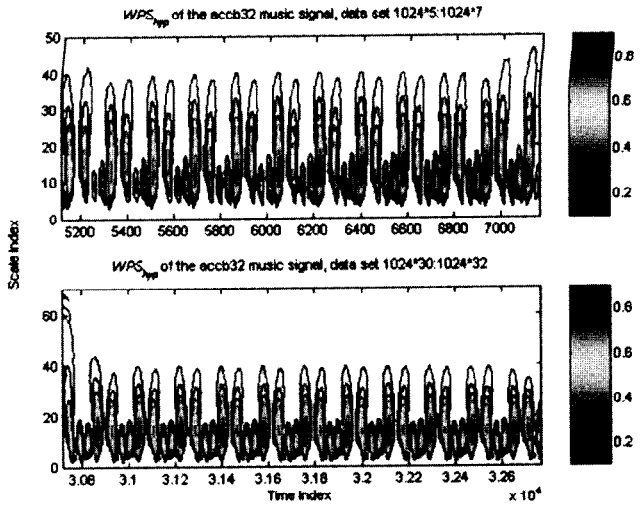

Fig. 26 Contour plots of the WPS_{hyp} of the accordion music signal of the two data sets.

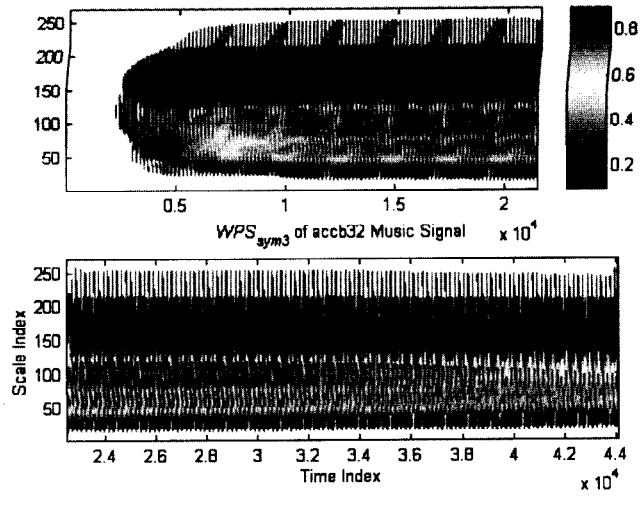

Fig. 27 Contour plot of the WPS_{sym3} of the accordion music signal for the time index from 1 to 44,100.

As we can see from Figs. 24 and 25, the 2048-sample music sets seem to exhibit periodic behavior in which their WPSs show repetitive energy patterns over time. The energy is mainly concentrated at the harmonic peaks and there are three subharmonics that can be clearly identified. This information can be used to classify the specific characteristics of the accordion signal. Thus, sounds from different musical instrument can be distinguished by examining their WPSs. The WPS_{hyp} of the accordion music signal of the previous data sets are given in Fig. 26.

As we can see from Fig. 26, the hyperbolic WPSs of the accordion music signal are consistent with the WPS_{sym3} given in Figs. 24 and 25 in which instantaneous periodic characteristics of the signal are successfully detected with bounded contours and repetitive patterns. The WPS_{hyp} and WPS_{sym3} are both very similar, which suggests that this music signal can be effectively studied using the hyperbolic and sym3 WPS techniques. From simulations, since the WPSs of various sets of the signal are very similar, it might be suggested that the musical accordion signal is periodic. To validate this conclusion, the WPS_{sym3} of the entire music signal is calculated and given in Fig. 27.

As we can see from Fig. 27, there are three main peaks present in the wavelet power spectrum of the signal. For the first 30,000 samples, periodic behavior is dominant as the peaks are clearly shown and the signal energy is evenly distributed, as seen in the time-index magnified versions of Fig. 27, which are Figs. 24 and 25. The third peak (located at the scale $a \approx 80$) disappears after the first 30,000 samples and there is uneven matching in energy distribution between the two strongest peaks (approximately located at scales of 60 and 100), which reflects the instability of the signal. From Figs. 27 and 34 in Sec. 7.2 (Fourier power spectrum of the accordion signal) it might be suggested that the music signal has entered into the chaotic region due to its broad and continuous Fourier power spectrum and uneven energy density as the time index increases.

The WPS_{hyp} of the accordion music signal, given in Fig. 28, agrees with the WPS_{sym3} given in Fig. 27 in which both wavelets can detect instantaneous periodic characteristics of the signal by having high contour scales. Note that the compression ratio of about $250/38 \approx 6.5$ is observed in Fig. 28, which results in a smaller scale range in this figure. From Fig. 28, the WPS_{hyp} consists of energy-density layers (approximately having the same center) at different scales. Especially, the harmonic peak (represented by the innermost layer) approximately terminates at the time index $b \approx 30{,}000$, which reflects the discontinuity of this musical signal. Other harmonic peaks (at lower scales due to a brighter color on the color scale) of the signal subsequently terminate at the time indices of 35,000 and 38,000. However, the subharmonic peaks (at very low scales) are present in the WPS_{hyp} for all time indices. As seen from Figs. 27 and 28, the WPS of the accordion signal varies for different values of time index, i.e., harmonic peaks decay over time, which indicates uneven energy density and discontinuity in the signal. In addition, different segments of the signal, which were recorded from one musical instrument, have different WPSs. Thus, although the signal ap-

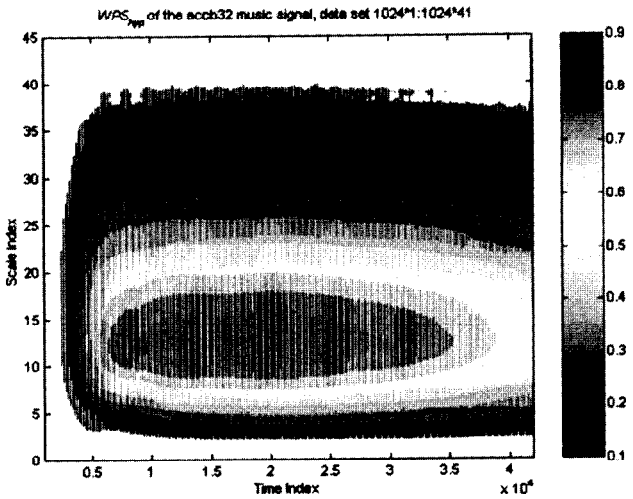

Fig. 28 Contour plot of the WPS_{hyp} of the accordion music signal.

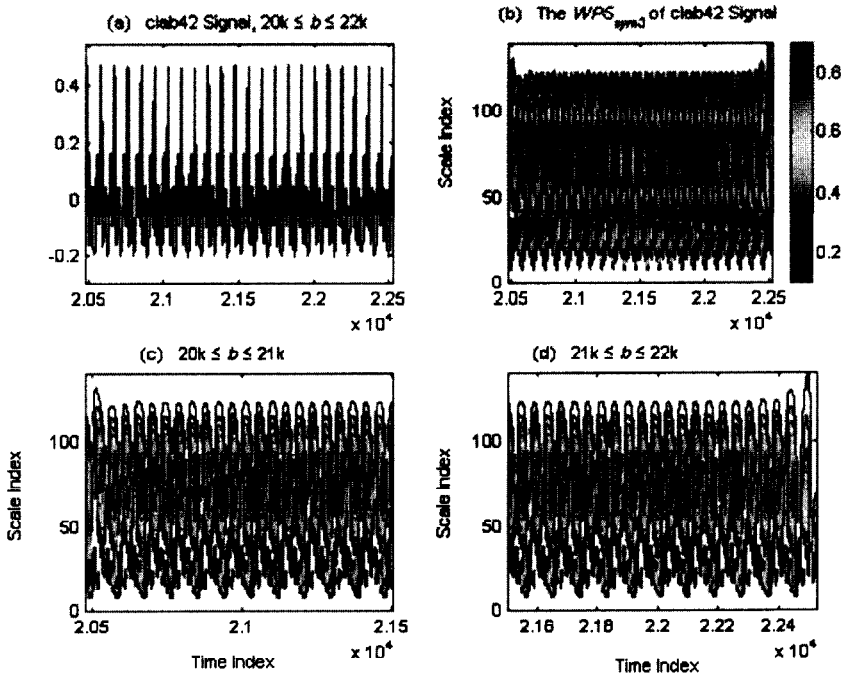

Fig. 29 Time-domain waveform (a) of the clarinet music data samples from 1024×20 to 1024×22 samples and contour plot of its WPS_{sym3} (b). The magnified contour plots of WPS_{sym3} are given in (c) and (d).

pears to be periodic in its time-domain waveforms, it is disordered or chaotic, as it has been shown in this paper and in other findings.[39–43]

7.2 *WPS of a Clarinet Music Signal*

The WPSs of various segments of the clarinet signal are given in Figs. 29 and 30. The first data set is chosen from the 1024×20 sample to the 1024×22 sample. As we can see in Fig. 29, the WPS consists of two distinctive peaks, which suggest that this set of the signal is periodic. There are two harmonic peaks and three subharmonics in "one period" of the waveform of about 80 samples or 1.8 ms. In Figs. 29(c) and 29(d), the peaks (which can be identified by high contour scales in the graph) are located at the scale of

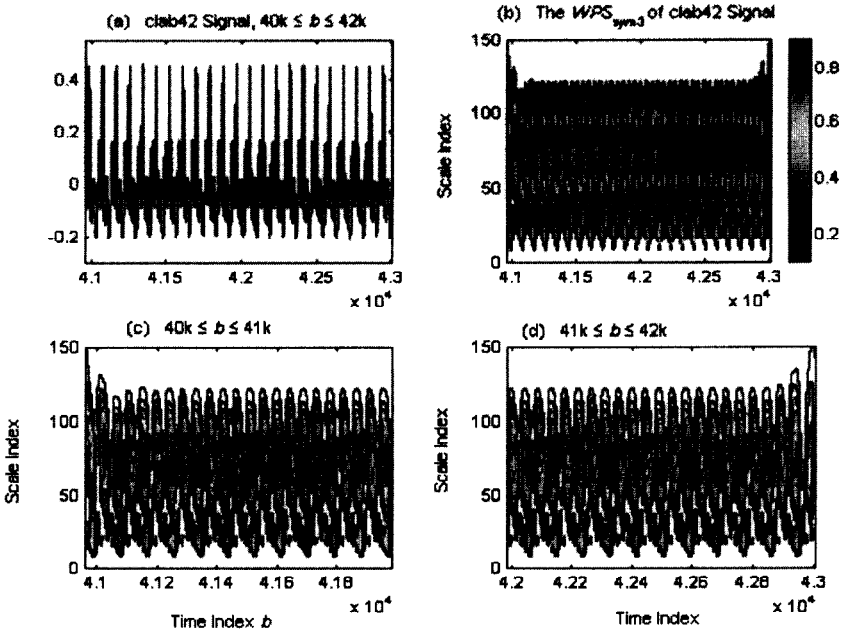

Fig. 30 Time-domain waveform of the 1024×40 to 1024×42 samples (a) and contour plot of WPS_{sym3} (b) of the clarinet musical signal. The magnified graphs of (b) are given in (c) and (d).

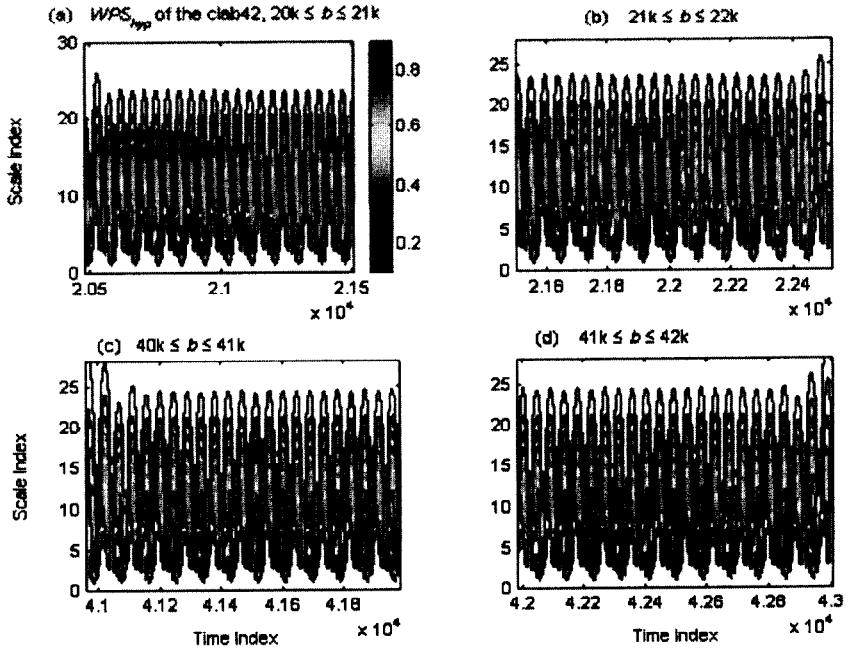

Fig. 31 Contour plots of the WPS_{hyp} of two separate sets of the clarinet music signal. The time index is expanded so that the WPS_{hyp} can be clearly displayed.

$a \approx 70$ and the subharmonics at the scale of $a \approx 20$. There is also continuity of energy because one peak and one subharmonic are located at the same time index.

The second data set is chosen from the 1024×40 sample to 1024×42 sample. This set, as seen in Fig. 30, exhibits similar characteristics to those of the first set, except that the energy concentration at the main harmonic peak is reduced due to a lower contour scale. The energy patterns of the harmonics and subharmonics are unchanged. The WPS_{hyp} of two separate data sets 1024×20:1024×22 and 1024×40:1024×42 are given in Figs. 31(a), 31(b), 31(c), and 31(d), respectively.

The WPS_{hyp} of this data set is consistent with its WPS_{sym3} in which major harmonic and subharmonic peaks are successfully detected. However, as seen from Fig. 31, the WPS_{hyp} cannot display some subharmonics of the clarinet music signal as it can in the case of the accordion signal. The WPS_{sym3} successfully displays all fine details of the signal, as we can see in Fig. 29. This is one disadvantage of the hyperbolic wavelet compared with the sym3 wavelet. However, the WPS_{hyp} is compressed to the highest scale of 25, which is about six times smaller than that of the WPS_{sym3}. Thus, calculation time of the WPS_{hyp} can be significantly reduced, which makes it more efficient than the WPS_{sym3}.

From Fig. 32, the WPS_{sym3} shows early "periodic" behavior due to high-contour color scales of the energy density, which represents one rapidly decaying peak. This can be understood as a burst of energy or an abrupt change in the signal energy. After that, there is no major harmonic peak in the signal and subharmonic peaks at low-contour scales, indicated by blue areas on the graph, which correspond to the maximum scale of 0.3, are dominant. At the sample 15,000, a change in energy is detected. From the time index of 25,000 onward, subharmonics are discontinued and they completely terminate at the time index $b \approx 37{,}000$. This might suggest that the signal is disordered since its components vary in a disorderedly manner with time. The contour scale of this figure is similar to that given in Fig. 30. Figure 33 displays the WPS_{hyp} of the clarinet music signal. From Figs. 32 and 33, it can be suggested that the hyperbolic and sym3 wavelets can successfully detect early periodic characteristics of the clarinet music signal. Then, periodicity decays away, which causes the WPSs of subsequent segments of the waveform to be unsymmetrical. Similar to the accordion musical signal, different segments of the clarinet music signal have different WPSs, which reflects its disordered characteristics. Section 7.1 and this section investigated the characteristics of two different mu-

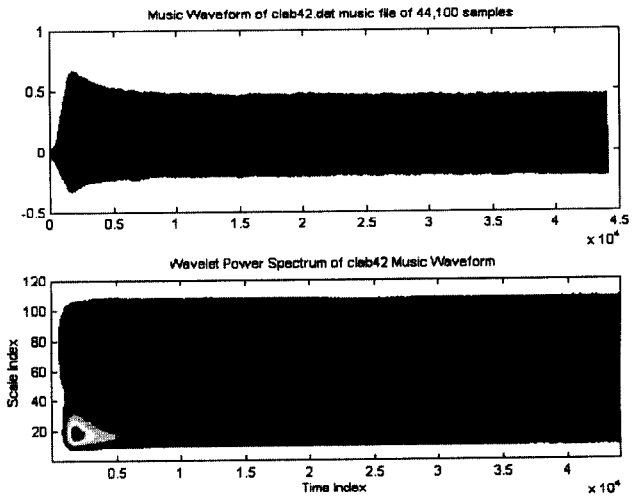

Fig. 32 Time-domain waveform and contour plot of the WPS_{sym3} of the clarinet signal.

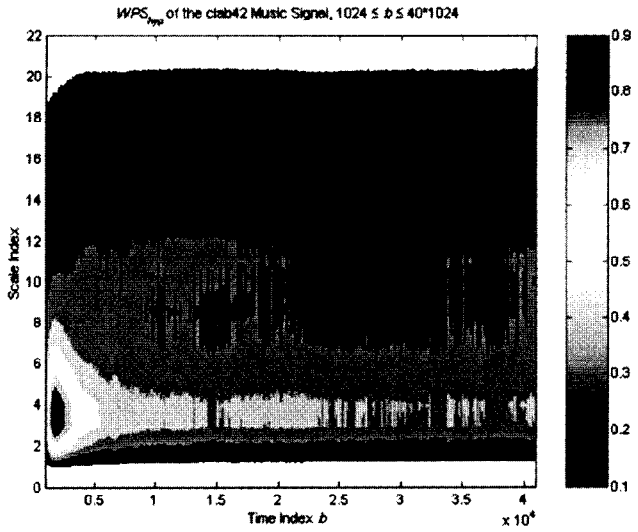

Fig. 33 Contour plot of the WPS_{hyp} of the clarinet music signal. Periodic components are clearly displayed in the scale range of 1 to 8 compared with 10 to 30 in Fig. 32.

sical signals, accordion and clarinet, using the hyperbolic and sym3 WPS techniques in which the disordered characteristics of both signals have been successfully revealed. Their WPSs were instantaneously displayed so that their behavior could be effectively monitored. The results found in this paper also agree with results found by other researchers.[35,39–43] The Fourier power spectra of music signals are given next to validate the results drawn by using the WPS technique.

From Fig. 34, we can be seen that the Fourier power spectrum of the accordion signal is broad with harmonic peaks over the low-frequency range. These peaks, as explained before, are fundamental components of the signal. The true behavior of the signal is based on the high-frequency components. In this case, the high-frequency spectrum is broad, which suggests that the signal exhibit chaotic behavior. The power spectrum of the clarinet music

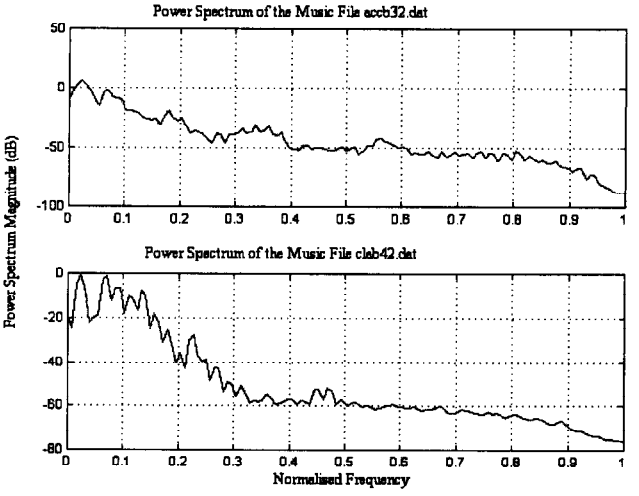

Fig. 34 Fourier power spectra of the accordion and clarinet music signals. The true maximum frequency of both the accordion and clarinet signals is 22.5 kHz.

signal has more distinctive periodic peaks than that of the accordion signal, which means that the former is more stable than the latter. Over the high-frequency range, the power spectrum is broad (as it was the case for the accordion signal), which suggests that the clarinet music signal might exhibit chaotic behavior. However, due to a large amount of periodic components over the low- and midfrequency ranges, chaotic behavior might not be dominant, and the signal, in this case, can be said to be in a transition to chaos.

In this section, the Fourier power spectrum technique has been successfully used to study characteristics of musical signals. It is clear that the WPS technique and Fourier power spectrum technique are consistent. However, compared with the WPS, the Fourier technique does not show instantaneous behavior of the signals over time. This is the disadvantage of the Fourier power spectrum technique since different segments of music signals have different power spectra. Thus, even though the Fourier technique can be used to study music, it is not effective compared with the WPS technique in this aspect. Recall that the WPS was not an effective tool to study an exponentially decaying sinusoidal signal and the ECG but the Fourier technique was. Therefore, depending on the input signal, the appropriate technique is chosen. For unknown signals, which are often encountered in practice, both techniques should be employed so that the most suitable technique can be identified.

By studying the instantaneous characteristics of musical signals using the hyperbolic WPS technique, it is possible to classify different musical sounds. The hyperbolic wavelet power spectrum technique gives locations in time (time index b) and frequency (inverse of the scale a) of harmonic and subharmonic peaks, which are unique for every signal. This is the major advantage of the WPS technique over the statistical technique,[34,35,37,39–43] the Wigner–Ville time-frequency power spectrum and the time-frequency STFT techniques.[33] The hyperbolic WPS technique has been shown to be an effective tool that promises useful applications in nonstationary signal classification. The main limitation on the time-frequency hyperbolic WPS technique is that for some signals, i.e., the ECG and the exponentially decaying sinusoid with a nonzero final value studied in Sec. 4, their WPSs are similar, even though their harmonic peaks are located at different scales. This makes the classification process of the two signals difficult. Another limitation is that the hyperbolic WPS is intensive to compute and thus powerful computing tools are required to improve the computation speed. This issue should be dealt with using parallel computation techniques.[44]

8 WPSs of Speech

Speech signals are examined in this section using both the WPS and the Fourier power spectrum techniques. Speech signals have been studied using time-frequency power spectrum analyses to detect formants over time.[21,45,46] Some popular kernels that have been used to study speech signals are the cone-shaped kernel,[46] Choi-Williams,[47] and signal-dependent Gaussian-shaped kernels.[8,20] This section attempts to study characteristics of speech signals using the new hyperbolic wavelet and the sym3 wavelet to detect periodic and chaotic behavior. The speech signals in this

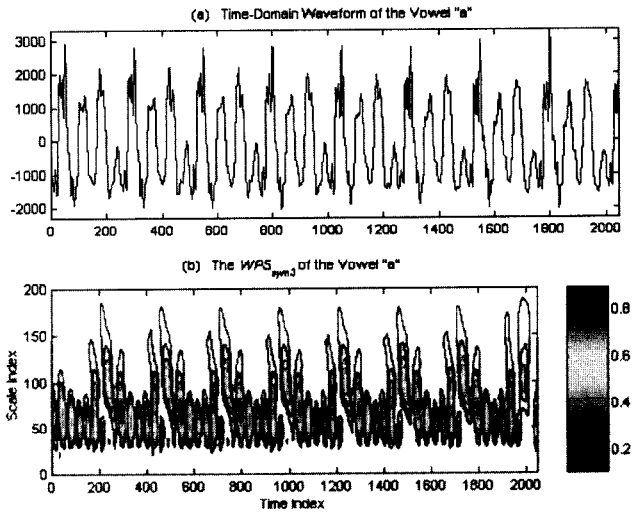

Fig. 35 The speech time-domain waveform of the vowel "a" and contour plot of its WPS_{sym3}.

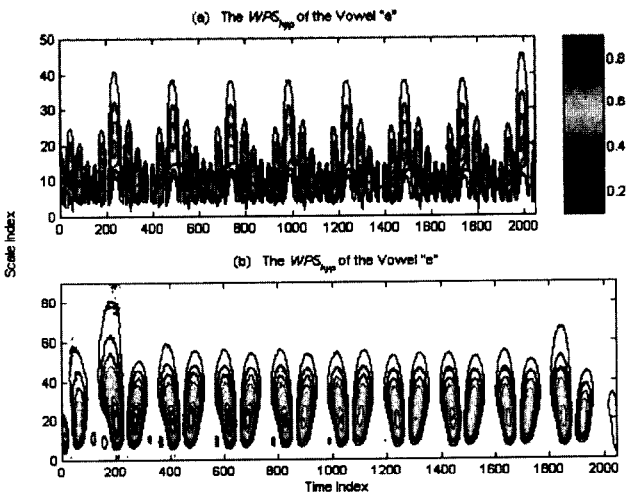

Fig. 37 Contour plots of the WPS_{hyp} of the speech vowels "a" and "e".

section are of 4096-samples long and they are the English vowels "a", "e", "i", "o", "u", and the sound "sh". Figure 35 shows the time-domain signal and the WPS_{sym3} of the vowel "a".

This speech signal exhibits strong periodic behavior by having a concentrated energy density at the peaks. Periodicity is strongly indicated by repetitive islands of closed contour curves in the WPS of the signal. Each harmonic peak is surrounded by a large number of subharmonics. The waveform seems to indicate periodic behavior although the energy is not completely discrete as compared with the sinusoidal signal in Sec. 2. Also note that there are no subharmonics associated with a harmonic peak simultaneously in time as it was the case for the clarinet music signal studied in Sec. 7.1. Thus, chaotic behavior does not exist in this speech waveform. The WPS_{sym3} of the vowel "e" is given in Fig. 36. The speech signal of the vowel "e" is genuinely considered periodic because of its uniform energy distribution and repetitive energy patterns over time. The peaks are clearly displayed and their scale index location is almost unchanged. There are two main peaks in "one period" of the WPS_{sym3} of the signal, which makes it significantly different from the vowel "a". This might suggest that the vowel "e" is more difficult for speech recognition due to its nonsubharmonics characteristics. The time-index magnified WPS_{hyp} of the vowels "a" and "e" are given in Figs. 37(a) and 37(b), respectively, which clearly show periodic peaks and subharmonics in the signals. These were also successfully detected by the sym3 wavelet. However, due to its compression effects compared with the WPS_{sym3}, the WPS_{hyp} could not clearly display the subharmonics, as can be seen in Figs. 37(b) and 36(b) for the vowel "e", which was reported earlier. Figure 38 shows the WPS_{sym3} of the vowel "i".

As can be seen from Fig. 38, the first part of the speech signal, which corresponds to the time index of less than 1600, exhibits periodic behavior, although "minor" chaotic

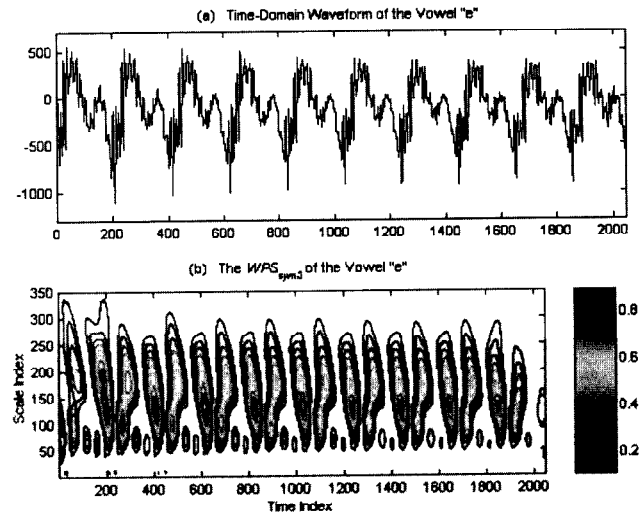

Fig. 36 Speech waveform of the vowel "e" and contour plot of its WPS_{sym3}.

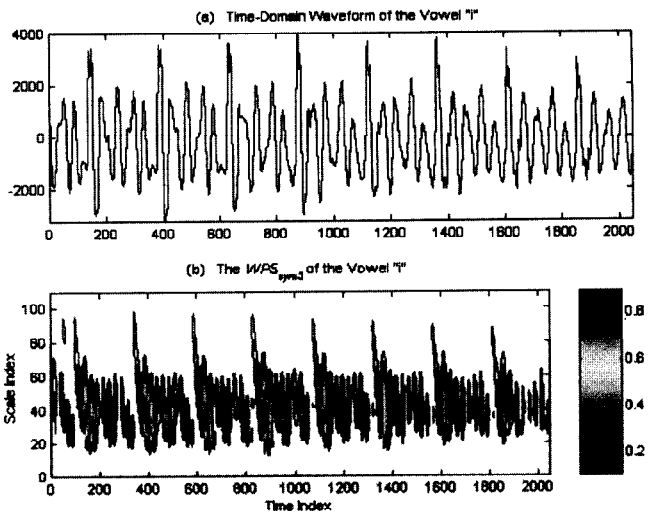

Fig. 38 Speech time-domain waveform of the vowel "i" and contour plot of its WPS_{sym3}.

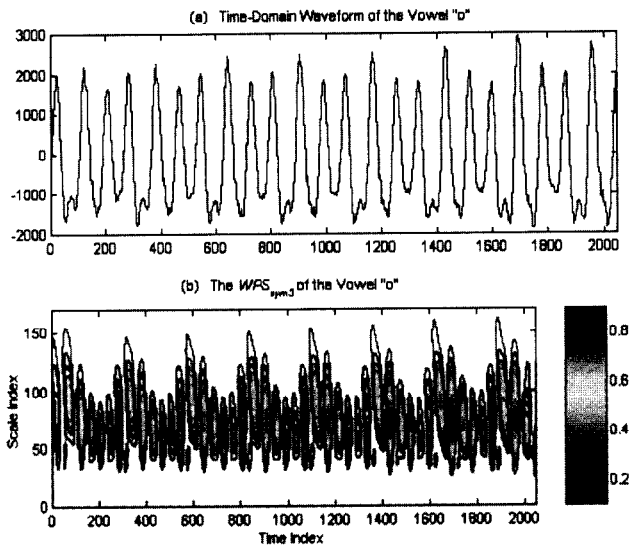

Fig. 39 Speech time-domain waveform of the vowel "o" and contour plot of its WPS_{sym3}.

behavior is indicated by its broad energy distribution at a low contour scale. In the second part of the waveform, which corresponds to the time index of greater than 1600, fundamental harmonics are not fully displayed but only the subharmonics at low contour scales. Although the majority of harmonics (contours at high scale) disappear from sample 1600 onward, the subharmonics (contours are at low scales) of the signal are still repetitive at regular time intervals. In addition, the occupied scale range of 20 to 100 of the energy distribution is short, which indicates strong periodicity in the signal. These two points suggest that the signal is periodic. This phenomenon, however, does not indicate chaos but indicates a change in the speech components of the signal which can be seen by changes in the time-domain waveform. The contour plot of the WPS_{sym3} of the vowel "o" is displayed in Fig. 39.

For the speech signal of the vowel "o", the flow of energy from sample 1500 onward indicates a change in its components in which the scale range slightly changes and the number of subharmonics decreases as the time index increases. The energy distribution of the signal is repetitive over regular time intervals, which might suggest that the signal is largely dominated by periodic components. Also note that the occupied scale range of the energy distribution is short, which indicates strong periodicity, as was the case of the vowels "a", "e", and "i" investigated earlier. The energy concentration at the peaks remains almost unchanged which further validates the preceding statement. The WPS_{hyp} of the vowels "i" and "o" are shown in Figs. 40(a) and 40(b), respectively.

As expected, the WPS_{hyp} of the vowels "i" and "o" are consistent with the WPS_{sym3} given in Figs. 38 and 39 in which periodicity is successfully detected. The energy patterns of the vowels "i" and "o", which are shown by using the hyperbolic wavelet, are consistent with those obtained by using the sym3 wavelet. The occupied scale ranges of the WPS_{hyp} of the vowels "i" and "o" are short, which once again indicates strong periodic characteristics. Note also that there are no changes in the scale range of the

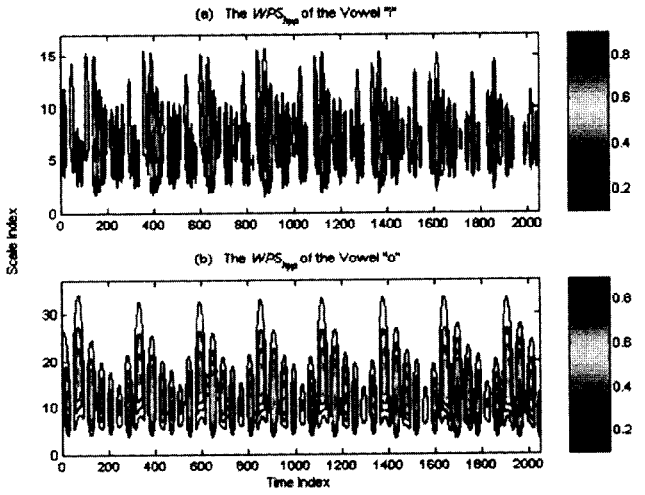

Fig. 40 Contour plots of the WPS_{hyp} of the speech vowels "i" and "o".

spectral components of the WPS_{hyp} of the vowels "i" and "o", as it is the case for the WPS_{sym3}. This is an ad 'antage of the hyperbolic wavelet to the sym3 wavelet, which is mainly due to its perfect symmetry. Note also that if the energy density of a signal is distributed over a narrow scale range and even though there is component variation in the signal, the signal is likely not chaotic, since its energy is not broadly distributed. This fact should be clearly understood since there are a number of signals that have component-variation characteristics, however, are not chaotic. The WPS_{sym3} of the vowel "u" is given in Fig. 41.

The WPS_{sym3} of the vowel "u" is discrete in which fundamental peaks at high contour scales are clearly shown, which shows strong periodicity in the signal. This signal can be regarded as similar to Duffing period 1 waveform except that there are three subharmonics associated with the main harmonic located at the approximate scale of 100. The

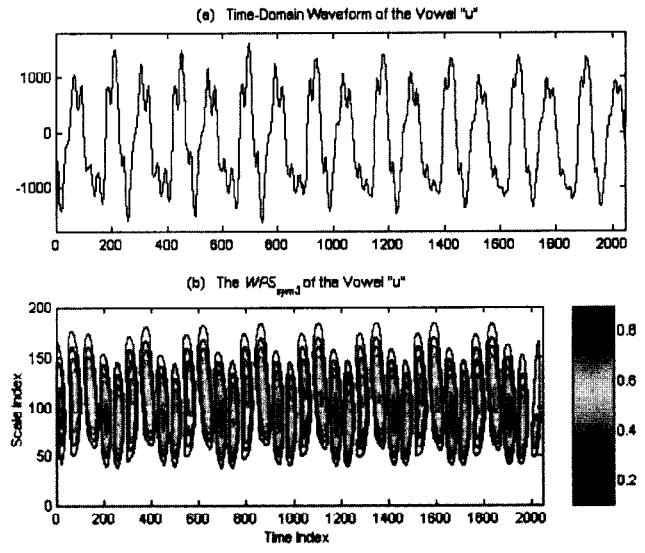

Fig. 41 Speech time-domain of the vowel "u" and contour plot of its WPS_{sym3}.

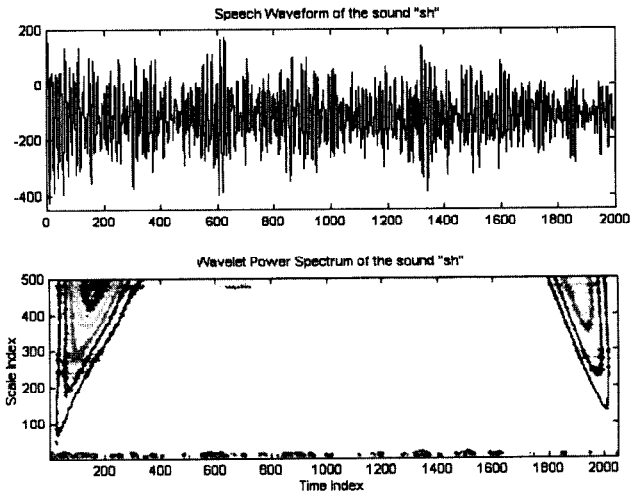

Fig. 42 Speech time-domain waveform of the sound "sh" and contour plot of its WPS_{sym3}.

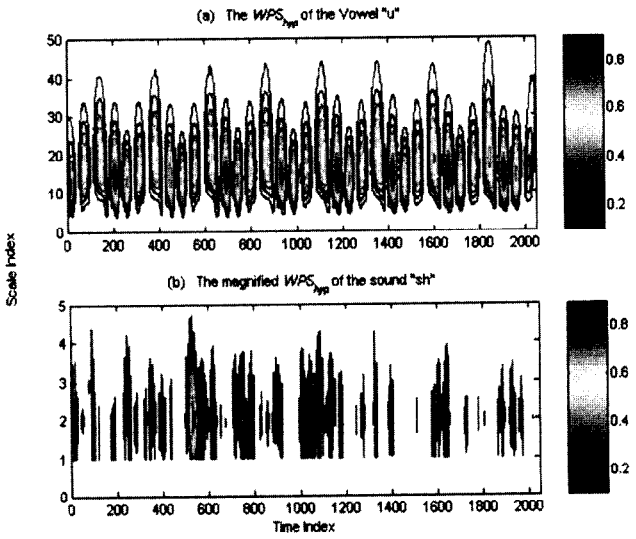

Fig. 44 Contour plots of the WPS_{hyp} of the speech vowel "u" and the speech sound "sh".

energy distribution is repetitive over regular time intervals. The WPS_{sym3} of the vowels "u" and "e" (given in Fig. 36) are similar in which both wavelet power spectra do not consist of subharmonics, which might suggest that they are difficult for speech recognition. The contour plot of the WPS_{sym3} of the "sh" sound is given in Fig. 42 and the magnified plot is given in Fig. 43. Figures 42 and 43 have identical contour scales.

The sound "sh", due to its nature, is very fast and noisy. As can be seen from Fig. 42, the usual discrete spectral components, as seen from the previous cases, disappear. Instead, there appears chaotic behavior similar to Duffing period 4 and Duffing chaotic waveforms studied in Secs. 5.3 and 5.4. However, harmonic peaks at very high scales (about larger than 500) are detected as can be seen in Fig. 42, which suggests that the signal is not chaotic. The main characteristics of the signal are determined by the low-scale energy patterns whose magnified plot is given in Fig. 43 in which the energy is unevenly distributed at the beginning of the signal. The samples in the middle of the signal are partly periodic and chaotic and there are no repetitive patterns in the WPS. This might suggest that the waveform is not periodic as it is usually the case for speech signals.

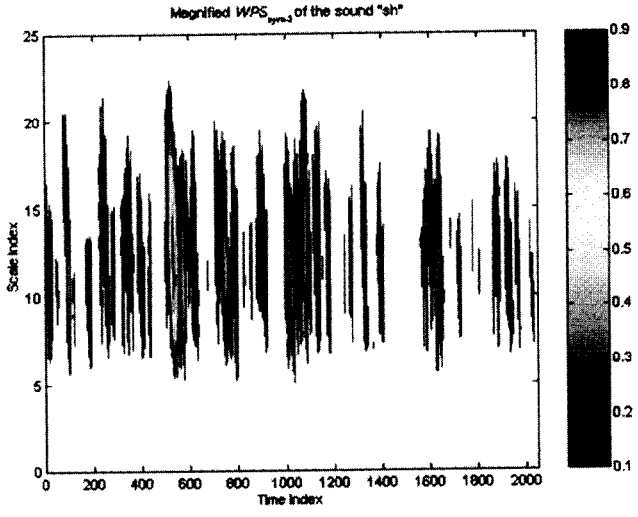

Fig. 43 Magnified contour plot of the WPS_{sym3} of the speech sound "sh".

A comparison of Fig. 43 with Fig. 17 (Duffing chaotic waveform) shows that the "sh" sound speech signal is not chaotic since its energy patterns are sharp and discontinuous, whereas the Duffing chaotic energy patterns are smooth. The sharp and fast-rising energy patterns of the "sh" sound signal do not indicate chaotic behavior, but instead, indicate considerable subharmonics variation in the waveform. The fundamental peak of the sound at a high contour scale of $a \approx 500$ (Fig. 42) is still present at $b \approx 550$, which validates the preceding suggestion that this signal is periodic, i.e., energy is still distributed at one scale of $a = 500$ and at a lower scale of $a = 10$ at intervals of $b = 550$, 1100, 1650, etc., as can be seen in Fig. 43. In addition, the scale range of this speech is short, which strongly suggests that it is not chaotic. The wavelet power spectrum of the sound "sh" is similar to that of the vowel "i" (but having fewer harmonic peaks) in which spectral component-variation is present. Contour plots of the WPS_{hyp} of the vowel "u" and the sound "sh" are shown in Figs. 44(a) and 44(b), respectively.

The WPS_{hyp} of the vowel "u" is similar to the WPS_{sym3} in which three associated subharmonics are detected. Although periodic peaks are not clearly presented in the WPS_{hyp}, the speech "sh" waveform is not chaotic since its energy distribution is not smooth and distributed over a narrow scale range, as can be seen in Fig. 44(b). The energy of the "sh" sound signal appears to flow in bursts at uneven time intervals which means there is component-variation in the signal. The new WPS technique, in particular using the hyperbolic and sym3 wavelets, has been effectively used to study speech signals. It has been shown that true characteristics of various musical and speech signals can be effectively studied by examining their hyperbolic and sym3 WPSs. The Fourier power spectrum technique is now employed to examine these signals so that the

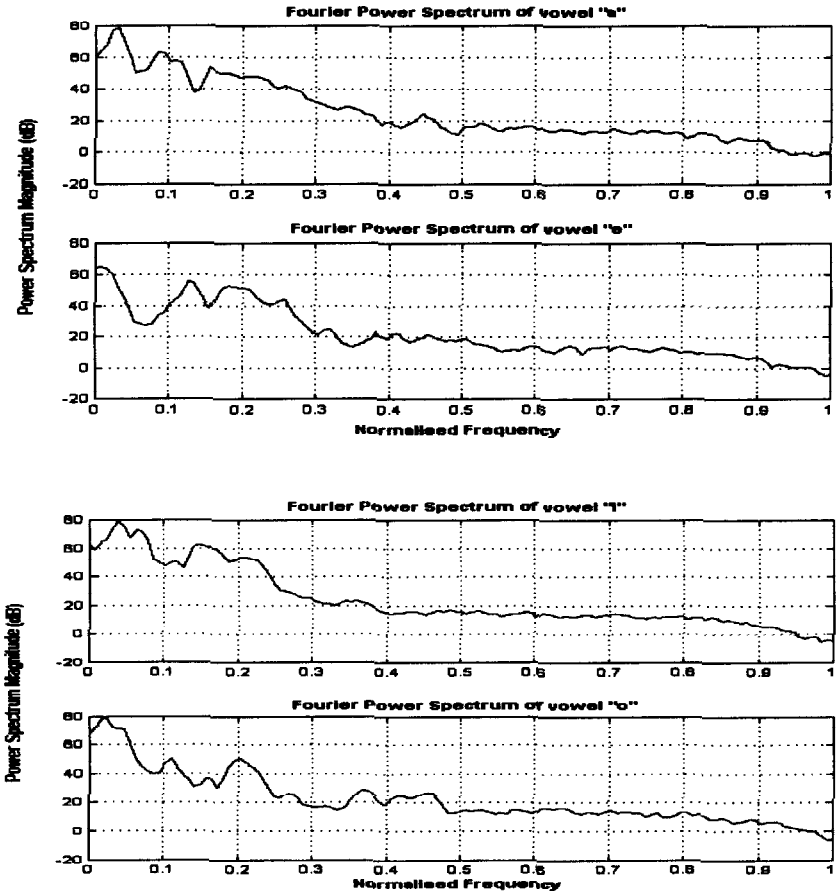

Fig. 45 Fourier power spectra of the vowels "a", "e", "i", and "o".

effectiveness of each technique can be clearly identified. The Fourier power spectra of all the speech vowels and the sound "sh" are shown in Figs. 45 and 46, respectively.

As can be seen from Figs. 45 and 46, the Fourier power spectra of speech signals exhibit distinctive peaks, which suggests that they are periodic. This conclusion is consistent with the results obtained using the WPS technique. The "sh" sound, although has a broad Fourier power spectrum, still does have one distinctive peak at a high contour scale. Evidently, by using the Fourier power spectrum technique, it is not possible to detect instantaneous behavior of the signal as it can be done using the WPS technique. This makes the WT method more applicable and effective than the Fourier transform method.

9 Remarks

Seven different signals have been studied in detail in this paper including a sinusoid, an exponential transient, an exponentially decaying sinusoid with a zero and nonzero dc component, Duffing oscillator, the ECG, music, and speech. We employed contour plots of their wavelet power spectra to recognize the presence of periodic, transient, and chaotic characteristics. The following remarks are drawn from the numerical simulation and analysis in this paper

1. If the contour plot of the WPS consists of a repetitive and discrete sequence of islands of closed and filled contour curves at high scales, then it is effectively periodic. Typical examples are a sinusoidal signal in Sec. 2, Duffing period 1 and 2 waveforms in Sec. 5, speech signals in Sec. 8. Music hyperbolic wavelet power spectra are repetitive locally, however, the energy pattern changes over the time index.
2. If the contour plot of the WPS consists of one peak and the contour curves have very large radii, which indicate a slow converging rate, then it is of a transient type. A typical example is an exponential signal in Sec. 3. If a small number of islands of distinctive closed contour curves are present, then the signal is transient-periodic, e.g., an exponentially decaying sinusoid with a zero final value in Sec. 4.
3. If the contour plot of the WPS consists of bounded contour curves with large radii (these radii are smaller than those discussed in case 2) then the signal is either transient-periodic (quasi periodic), e.g., an exponentially decaying sinusoid with a nonzero dc component in Sec. 4, or chaotic, e.g., the ECG. To differentiate between these two cases, the occupied scale ranges of their WPSs are used.
4. If the WPS of the signal covers a large scale range (approximately larger than 2000 scales), then the signal is chaotic, e.g., the ECG. Otherwise, it is transient-periodic.
5. If the WPS is continuous (ECG signal) and there are changes in its energy patterns, i.e., the energy distri-

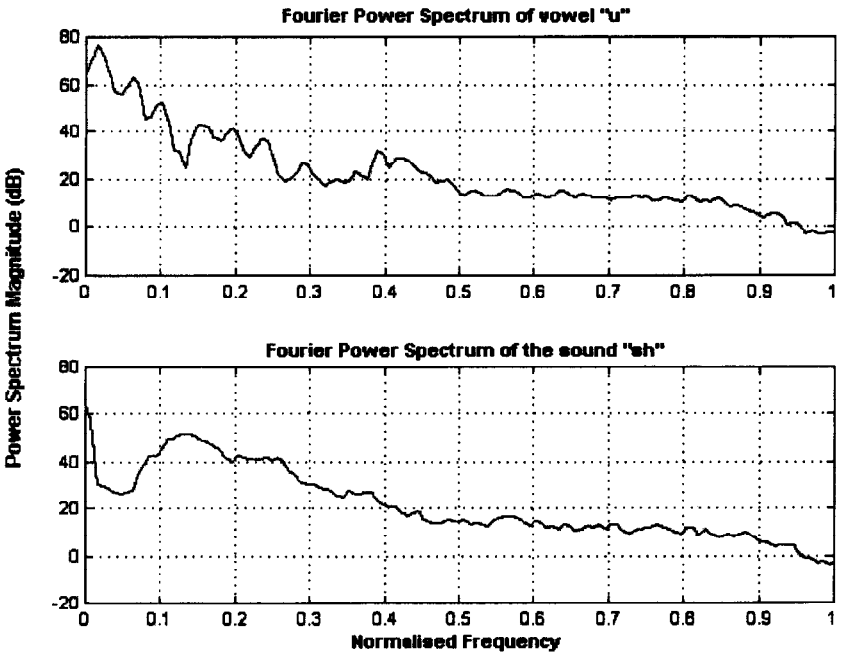

Fig. 46 Fourier power spectra of the vowel "u" and the sound "sh". The frequency of each signal is normalized by dividing every frequency bin by the largest frequency bin of the signal spectrum. Thus, the shape of the power spectrum will not be changed by the normalization process.

bution varies for different data segments, that means the signal is possibly in the transition into the chaotic region, e.g., Duffing period 4 waveform and music in Sec. 7.

6. If the contour plot of the WPS is nonrepetitive and contour curves have low scales, then the signal has entered into the chaotic region, e.g., Duffing chaotic waveform. Note that for cases 4 and 5, the occupied wavelet power spectral scale range of the signal is wide and its energy density is broad and continuous.

10 Conclusions

The contribution of this paper is to establish a gallery of the proposed WPS_{hyp}. Seven signals were examined including a sinusoid, an exponential transient, an exponentially decaying sinusoid with a zero and nonzero dc component, a Duffing oscillator, the ECG, music, and speech. The Fourier power spectra of these signals were also displayed and compared with their hyperbolic WPSs. The Duffing oscillator was examined in detail and the observed results are consistent with previous results reported in the literature. The ECG signal appears to exhibit chaotic behavior in which smooth, broad, and no major harmonic peaks were detected in its WPS. Music signals behave chaotically even though the WPSs of different sets of the signals appear to be instantaneously periodic. This can be explained by the fact that harmonic peaks of musical signals abruptly disappear over time, which reflects the disordered characteristics of these signals. The findings in this paper agree with results found by other researchers.[33–35,37,39–43] Speech signals were found to be periodic with strong harmonic peaks and several subharmonics. It was shown that remarks drawn by using the WPS and Fourier power spectrum techniques are consistent. Some speech signals exhibit component variation but they are not chaotic since their wavelet power spectra are not broad and occupy narrow scale ranges. The WPS technique seems to be more effective than the Fourier power spectrum technique in studying music and speech signals. Although the WPS technique has the advantage (over the Fourier technique) of showing signal energy distributions in time and frequency domains, it is not effective when examining the ECG signal. In fact, the WPS_{hyp} and WPS_{sym3} of the ECG and the exponentially decaying sinusoid with a nonzero dc component signals were almost identical. In contrast, the Fourier power spectra of these signals can be differentiated which is the disadvantage of the WPS technique. The hyperbolic wavelet has also been shown to be more effective than the sym3 wavelet in terms of having a smaller total number of scales, which results in less computational burden. In addition, the hyperbolic wavelet also can detect energy components at very low scales. However, the sym3 wavelet is more effective when displaying fine subharmonics, as was seen in cases of speech signals. Early results of signal analysis presented in this paper using the hyperbolic WPS technique form a foundation for future quantitative work including comparisons of the new technique with other techniques, quantitative studies of the ECG for medical purposes, and more detailed and advanced work on music and speech signals for pattern recognition.

Acknowledgments

We are very grateful to the reviewers for their useful comments, which significantly improved the quality of the paper. The first author would like to thank Department of Electrical and Computer Systems Engineering, Monash University, Clayton campus for the 2002 Postgraduate Publication Award and its great support throughout the years.

References

1. C. L. Nikias and J. M. Mendel, "Signal processing with higher-order spectra," *IEEE Signal Process. Mag.* **10**(3), 10–37 (1993).
2. C. L. Nikias and M. R. Raghuveer, "Bispectrum estimation: a digital signal processing framework," *Proc. IEEE* **75**(7), 869–891 (1987).
3. J. M. Lipton et al., "Use of the bispectrum to analyse properties of the human electrocardiograph," *Australas. Phys. Eng. Sci. Med.* **21**, 1–11 (1998).
4. J. M. Lipton and K. P. Dabke, "Bispectra of non-linear systems," Report from the Department of Electrical and Computer Systems Engineering, Faculty of Engineering, Monash University, Clayton VIC (1994).
5. W. B. Collis, P. R. White, and J. K. Hammond, "Higher-order spectra: the bispectrum and trispectrum," *Mech. Syst. Signal Process.* **12**(3), 375–394 (1998).
6. V. Chandran and C. Pezeshki, "Bispectral and trispectral characterization of transition to chaos in the Duffing oscillator," *Int. J. Bifurcation Chaos Appl. Sci. Eng.* **3**(3), 551–557 (1993).
7. Y. C. Kim and E. J. Powers, "Digital bispectral analysis and its applications to nonlinear wave interactions," *IEEE Trans. Plasma Sci.* **PS-7**(2), 120–131 (1979).
8. L. Cohen, "Time-frequency distributions—a review," *Proc. IEEE* **77**(7), 941–981 (1989).
9. K. N. Le, K. P. Dabke, and G. K. Egan, "The hyperbolic kernel for time-frequency power spectrum," *Opt. Eng.* (in press).
10. M. D. Khac, C. Basdevant, V. Perrier, and K. D. Tran, "Wavelet analysis of 2-D turbulent fields," *Physica D* **76**(1–3), 252–277 (1994).
11. A. Kyprianou and W. J. Staszewski, "On the cross wavelet analysis of Duffing oscillator," *J. Sound Vib.* **228**(1), 199–210 (1999).
12. M. Farge, N. Kevlahan, V. Perrier, and E. Goirand, "Wavelets and turbulence," *Proc. IEEE* **84**(4), 639–669 (1996).
13. A. B. Doser, "Speech analysis for hearing impaired using chirped wavelets," in *Conf. Record of the 34th Asilomar Conf. on Signals, Systems and Computers*, Vol. 2, pp. 1494–1497 (2000).
14. I. Daubechies, *Ten Lectures on Wavelets*, pp. 1–16, The Society for Industrial and Applied Mathematics, Philadelphia (1992).
15. D. Coca and S. A. Billings, "Continuous-time system identification for linear and nonlinear systems using wavelet decompositions," *Int. J. Bifurcation Chaos Appl. Sci. Eng.* **7**(1), 87–96 (1997).
16. B. Celler, G. Y. C. Chung, and C. Phillips, "ECG analysis and processing using wavelets and other methods," *Biomed. Eng. Appl. Basis Commun.* **9**(2), 81–90 (1997).
17. C. S. Burrus, R. A. Gopinath, and H. Guo, *Introduction to Wavelets and Wavelet Transforms: A Primer*, pp. 10–50, Prentice-Hall, Englewood Cliffs, NJ (1998).
18. A. Bruce, D. Donoho, and H. Y. Gao, "Wavelet analysis," *IEEE Spectrum* **33**(10), 26–35 (1996).
19. A. Arneodo, "Wavelet analysis of fractals: from the mathematical concepts to experimental reality," in *Wavelet: Theory and Applications*, M. Y. H. and L. M. J. G. Erlebacher, Eds., pp. 349–493, Oxford University Press, Oxford (1996).
20. L. Cohen, "Introduction: a primer on time-frequency analysis," in *Time-Frequency Signal Analysis: Methods and Applications*, B. Boashash, Ed., pp. 3–43, John Wiley, New York (1992).
21. K. N. Le, K. P. Dabke, and G. K. Egan, "The hyperbolic wavelet function," in *Aerosense—Wavelet Applications VIII, Proc. SPIE* **4391**, 411–422 (2001).
22. B. P. van Milligen et al., "Wavelet bicoherence: a new turbulence analysis tool," *Phys. Plasmas* **2**(8), 3017–3032 (1995).
23. B. P. van Milligen, C. Hidalgo, and E. Sanchez, "Nonlinear phenomena and intermittency in plasma turbulence," *Phys. Rev. Lett.* **74**(3), 395–398 (1995).
24. B. A. Jubran, M. N. Hamdan, and N. H. Shabaneh, "Wavelet and chaos analysis of flow induced vibration of a single cylinder in cross-flow," *Int. J. Eng. Sci.* **36**(7–8), 843–864 (1998).
25. W. J. Staszewski and K. Worden, "Wavelet analysis of time-series: coherent structures, chaos and noise," *Int. J. Bifurcation Chaos Appl. Sci. Eng.* **9**(3), 455–471 (1999).
26. B. P. Lathi, *Signals, Systems and Communication*, pp. 14–152, 515–531, John Wiley and Sons, New York (1965).
27. R. M. S. S. Abeysekera and B. Boashash, "Time-frequency domain features of ECG signals: their application in P wave detection using the cross Wigner-Ville distribution," in *Proc. IEEE Conference on Acoustics, Speech and Signal Processing*, Vol. 3, pp. 1524–1527 (May 1989).
28. M. E. Tagluk and M. J. English, "The analysis of ECG signals using time-frequency techniques," in *Proc. 19th Int. Conf. IEEE Eng. Med. Biol. Soc.*, Vol. 3, pp. 1320–1323 (1997).
29. P. E. Tikkanen, J.-E. Palmgren, and L. C. Sellin, "Wavelet analysis of ECG and MAP signals," in *Proc. 19th Int. Conf. IEEE Eng. Med. Biol. Soc.*, Vol. 1, pp. 317–320 (1997).
30. I. Kaminskyj and A. Materka, "Automatic source identification of monophonic musical instrument sounds," in *Proc. IEEE Int. Conf. on Neural Networks*, pp. 189–194 (1995).
31. I. Kaminskyj and A. Materka, "Automatic monophonic musical instrument sound identification system," in *Proc. ACMA Conf.*, pp. 41–46 (1996).
32. I. Kaminskyj, "Multidimensional scaling analysis of musical instrument sounds' spectra," in *Proc. ACMA Conf.*, pp. 36–39 (1999).
33. C. Delfs and F. Jondral, "Classification of piano sounds using time-frequency signal analysis," in *Proc. IEEE Conference on Acoustics, Speech and Signal Processing*, Vol. 3, pp. 2093–2096 (1997).
34. K. N. Hamdy, A. H. Tewfik, T. Chen, and S. Takagi, "Time-scale modification of audio signals with combined harmonic and wavelet representations," in *Proc. IEEE Conference on Acoustics, Speech and Signal Processing*, pp. 439–442 (1997).
35. T. Lambrou et al., "Classification of audio signals using statistical features on time and wavelet transform domains," in *Proc. IEEE Conference on Acoustics, Speech and Signal Processing*, Vol. 6, pp. 3621–3624 (1998).
36. R. Sussman and M. Karsh, "Analysis and resynthesis of musical instrument sounds using energy separation," in *Proc. IEEE Conference on Acoustics, Speech and Signal Processing*, Vol. 2, pp. 997–999 (1996).
37. P. De Gersem, B. De Moor, and M. Moonen, "Applications of the continuous wavelet transform in the processing of musical signals," in *Proc. 13th Int. Conf. on Digital Signal Processing Proceedings*, Vol. 2, pp. 563–566 (1997).
38. G. Olmo, F. Dovis, P. Benotto, C. Calosso, and P. Passaro, "Instrument dependent analysis of music by means of the continuous wavelet transform," *Proc. SPIE* **3813**, 716–726 (1999).
39. N. H. Fletcher, "Inharmonicity, nonlinearity and music," *The Physicist* **37**(5), 171–175 (2000).
40. J. Jeong, M. K. Joung, and S. Y. Kim, "Quantification of emotion by nonlinear analysis of the chaotic dynamics of electroencephalograms during perception of 1/f music," *Biol. Cybern.* **78**(3), 217–225 (1998).
41. N. Birbaumer, W. Lutzenberger, H. Rau, and C. Braun, "Perception of music and dimensional complexity of brain activity," *Int. J. Bifurcation Chaos Appl. Sci. Eng.* **6**(2), 267–278 (1996).
42. M. Morando, G. Morgavi, and C. Martini, "Local prediction in musical time series," *Int. J. Model. Simulat.* **16**(1), 1–5 (1996).
43. A. S. Dmitriev, A. I. Panas, and S. O. Starkov, "Experiments of speech and music signals transmission using chaos," *Int. J. Bifurcation Chaos Appl. Sci. Eng.* **5**(4), 1249–1254 (1995).
44. K. N. Le, G. K. Egan, and K. P. Dabke, "Parallel computation of the hyperbolic time-frequency power spectrum: analysis and comparison to the bispectrum," in *Proc. ICII 2001 Conf. C*, pp. 322–327 (2001).
45. L. E. Atlas, P. J. Loughlin, and J. W. Pitton, "Signal analysis with cone kernel time-frequency distributions and their application to speech," in *Time-Frequency Signal Analysis: Methods and Applications*, B. Boashash, Ed., pp. 375–388, Longman, Cheshire (1992).
46. Y. Zhao, L. E. Atlas, and R. J. Marks II, "The use of cone-shaped kernels for generalized time-frequency representations of nonstationary signals," *IEEE Trans. Acoust., Speech, Signal Process.* **38**(7), 1084–1091 (1990).
47. H.-I. Choi and W. J. Williams, "Improved time-frequency representation of multicomponent signals using exponential kernels," *IEEE Trans. Acoust., Speech, Signal Process.* **37**(6), 862–871 (1989).

Khoa N. Le graduated with first-class honors in electrical and computer systems engineering and received his PhD in 2002 from Monash University, Clayton, Melbourne, Australia. He is currently a lecturer with Griffith University, Gold Coast, Queensland, Australia. His research interests are digital signal processing, time-frequency signal processing, parallel computing, telecommunications, and higher order spectrum.

Kishor P. Dabke graduated with BE(E) and ME(E) degrees from M. S. University of Baroda, India, and received his PhD degree from Monash University, Australia, where he has been with the Department of Electrical and Computer Systems Engineering since 1966, and is currently an honorary research associate. His research interests are control systems, nonlinear and chaotic systems and application of ES and artificial intelligence in engineering. He is a fellow of IE (India) and a member of IE (Australia) and IEEE.

Gregory K. Egan is currently a professor of telecommunications and information engineering. He directs the Center for Telecommunications and Information Engineering and heads the Department of Electrical and Computer Systems Engineering, Monash University, Australia. His research interests are the design, programming, and the application of high-performance parallel distributed computer architectures.